Use of Bayesian inference for parameter recovery in DC and AC Voltammetry.

Professor David J. Gavaghan[1,*], Dr Jonathan Cooper[1], Aidan C. Daly[1], Dr Christopher Gill[2], Dr Kathryn Gillow[3], Dr Martin Robinson[1], Dr Alexandr N. Simonov[4], Dr Jie Zhang[4], and Professor Alan M. Bond[4,*]

[1]Department of Computer Science, University of Oxford, Wolfson Building, Parks Road, Oxford, OX1 3QD, United Kingdom.
[2]Department of Statistics, University of Oxford 24-29 St Giles', Oxford, OX1 3LB, United Kingdom.
[3]Mathematical Institute, University of Oxford, Andrew Wiles Building, Radcliffe Observatory Quarter, Woodstock Road, Oxford, OX2 6GG, United Kingdom.
[4]School of Chemistry, Monash University, Clayton, Vic. 3800, Australia.
[*]Corresponding authors: david.gavaghan@cs.ox.ac.uk, alan.bond@monash.edu.au

September 7, 2017

Abstract

We describe the use of Bayesian inference for quantitative comparison of voltammetric methods for investigating electrode kinetics. We illustrate the utility of the approach by comparing the information content in both DC and AC voltammetry at a planar electrode for the case of a quasi-reversible one electron reaction mechanism. Using synthetic data (i.e. simulated data based on Butler-Volmer electrode kinetics for which the true parameter values are known and to which realistic levels of simulated experimental noise have been added), we are able to show that AC voltammetry is less affected by experimental noise (so that in effect it has a greater information content then the corresponding DC measurement) and hence yields more accurate estimates of the experimental parameters for a given level of noise. Significantly, the AC approach is shown to be able to distinguish higher values of the rate constant. The results of using synthetic data are then confirmed for an illustrative case of experimental data for the $[Fe(CN)_6]^{3-/4-}$ process.

1 Introduction

There are numerous voltammetric techniques and associated methodologies available for evaluating the electrode kinetics of a simple quasi-reversible reaction of the kind

$$A \underset{}{\overset{E_0,k_0,\alpha}{\rightleftharpoons}} B + e^-, \tag{1}$$

where species A and B are in solution, and E_0, k_0, and α are the reversible formal potential, standard heterogeneous charge transfer rate constant at E_0 and the charge transfer coefficient, respectively, assuming that the Butler-Volmer formalism is used to describe the electron transfer process [1, 2, 3]. With any voltammetric technique, the strategy adopted to determine the kinetics is to vary the external variable related to time (e.g. sweep rate in DC voltammetry, frequency in AC voltammetry, electrode rotation rate in hydrodynamic voltammetry). The direction and extent of variation of the voltammetric response on the relevant time domain provide the diagnostic criteria for establishing the type of mechanism involved. Analysis of the current-potential-time (frequency) relationships allow the magnitude of E_0, k_0 and α to be evaluated [1, 4, 2]. An upper limit on the measured k_0 values is reached when the quasi-reversible theory becomes experimentally indistinguishable from that predicted for a reversible i.e. a Nernstian process [5]. That is, when the electrode kinetics becomes sufficiently fast, the process obeys the laws of thermodynamics rather than kinetics so the response becomes independent of k_0 and α.

DC cyclic voltammetry is probably the most commonly used technique to determine k_0 values. With this method, in which the DC potential applied to the working electrode versus a reference electrode is cycled over a designated range at a known scan rate, v, it was demonstrated over 60 years ago that the shape of the voltammetric response and hence the kinetics are functions of a parameter Λ, defined as [6]

$$\Lambda = \frac{k_0}{(D_A^{1-\alpha} D_B^{\alpha} \phi v)^{\frac{1}{2}}}, \tag{2}$$

where D_A and D_B are the diffusion coefficients of the oxidised and reduced species and $\phi = F/RT$, where F is Faraday's constant, R is the universal gas constant, and T is the absolute temperature. Assuming, as is typically the case, that $D_A = D_B = D$, this reduces to

$$\Lambda = \frac{k_0}{(D\phi v)^{\frac{1}{2}}}. \tag{3}$$

These authors then introduced the concept of kinetic zone boundaries which they suggested could be summarized as

$$\begin{aligned}
&\text{Reversible (Nernstian)} && \Lambda \geq 15; k_0 \geq 0.3 v^{\frac{1}{2}} \text{cm s}^{-1} \\
&\text{Quasireversible} && 15 \geq \Lambda \geq 10^{-2(1+\alpha)}; 0.3 v^{\frac{1}{2}} \geq k_0 \geq 2 \times 10^{-5} v^{\frac{1}{2}} \text{cm s}^{-1} \\
&\text{Totally irreversible} && \Lambda \leq 10^{-2(1+\alpha)}; k_0 \leq 2 \times 10^{-5} v^{\frac{1}{2}} \text{cm s}^{-1},
\end{aligned} \tag{4}$$

assuming a temperature of 298 K.

Subsequently, it became widely recognized that the magnitudes of the non-faradaic terms of uncompensated resistance (R_u) and double layer capacitance (C_{dl}) and hence the cell time constant ($R_u C_{dl}$) provide significant constraints on the upper limit of k_0 that can be measured by DC cyclic voltammetry [1, 4]. Nevertheless, k_0 values of about 1 cm s^{-1} are accessible at very high scan rates ($>$ 10 kV s^{-1}) when using DC cyclic voltammetry with microelectrodes with molecular solvents containing sufficiently high concentrations of supporting electrolyte, and data when analysis is based on detailed comparisons of simulated and experimental data.

In the technique of electrochemical impedance spectroscopy (EIS) usually a sequence of phase-randomized small amplitude sine waves are superimposed onto the constant

potential. This method is also widely used to study electrode kinetics and generally employs data analysis based on equivalent circuits to evaluate E_0, k_0, α, R_u, and C_{dl}. Again, with this method, the conclusion has been reached that there is an upper limit of accessible k_0 values that can be defined semi-quantitatively . The highest value of ω or shortest time domain that can be used with EIS, where $\omega = 2\pi f$ (where f (Hz) is the frequency), is determined by the cell time constant which must remain much smaller than the cycle period of the applied AC waveform. Under these circumstances and with the diffusion coefficient $D_A = D_B = D$, the upper limit condition is given by $k_0 \leq (\frac{D\omega}{2})^{\frac{1}{2}}$ (see [1], page 387). Assuming that a frequency of 10 MHz can be used [7], so that $\omega = 10^7$ s^{-1} and using a value of $D = 10^{-5}$ cm^2 s^{-1} reveals that k_0 values in the 5 to 10 cm s^{-1} range should be accessible in aqueous electrolyte media, as indeed is the case [3].

In our laboratories we have expanded the use of AC voltammetry (whereby the linear sweep used in DC Voltammetry is augmented by the superimposition of a sinusoidally varying waveform) from its traditional small amplitude form to the case where the DC components are filtered out and the AC current displayed and analyzed as a function of DC potential [8] (as also effectively applies in EIS studies). By emphasizing the use of large amplitude sine waves superimposed onto the DC ramp, we have demonstrated that this approach provides access to even more powerful tools in quantitative electrode kinetics [9, 10, 7, 11, 12]. In one approach to electrode kinetic evaluation, the aperiodic DC component and higher order AC harmonics, that provide a key additional feature of this form of AC voltammetry, are resolved by Fourier transform methods as part of a data analysis strategy in which experimental and simulated data for individual harmonics are compared in order to determine values of R_u, C_{dl}, E_0, k_0 and α. Significantly [7, 10], the resolved higher order AC harmonics are devoid of the background capacitance current that can severely restrict the use of DC and small amplitude AC voltammetry. Alternatively the total current (DC plus AC) response derived from large amplitude AC voltammetry may be directly used in a comparison of simulated and experimential data without the need to introduce Fourier or any other form of analogue or digital filtering [13, 5]; this direct approach does however require that the model used to mimic the potential dependence of the double layer capacitance allows a sufficiently accurate representation of the experimental data to be achieved, or that the magnitude of the background double layer capacitance current is small, relative to the faradaic current that governs the electrode kinetics. The frequencies of the applied sine waves we have used in large amplitude AC voltammetry are usually much lower that the upper ones used in EIS and only in the 10 to 1000 Hz range. On the basis of the widely used time window and accessible rate constant argument used above it would therefore not be anticipated that under our low frequency conditions we would be able to measure k_0 values approaching the upper limits reported for DC cyclic voltammetry at microelectrodes with scan rates in the 10 kV s^{-1} region or by EIS with frequencies extending to the MHz region. The factor that comes into play with the AC voltammetric method in either Fourier or total AC current versions is not just the time window, but the very strong dependence of the magnitude of the AC current, particularly in higher order harmonics, on k_0 relative to the situation that applies in DC cyclic voltammetry. This kinetically sensitive current magnitude feature also is one that is not accessed in conventional forms of data analysis by EIS.

Having recognized on the basis of experimental observations that AC voltammetry can be far more sensitive to measurement of fast electrode kinetics than inferred on the basis of the time window and accessible rate constant type arguments [7], we now quantitatively explore the relative sensitivity of DC and AC voltammetry on a broader base of arguments. By introducing Bayesian inference methodology, we are able to demonstrate why

access to very much faster k_0 values is inherently possible when kinetic analysis utilizes direct comparisons of the current-potential-time (frequency) simulated and experimental responses. In order to provide a directly comparable evaluation of the relative kinetic sensitivity of DC and AC voltammetry, we have undertaken analysis of the mathematically purer total (AC plus DC) current version of the technique rather than analysis of Fourier transformed versions of the technique which by definition employ filtered data and reject noise [11] that introduce data enhancing characteristics not available in the DC method.

Mathematical Theory and Computational Methods

Background - Why Bayesian Methods?

Electrochemical measurement techniques are underpinned by mathematical models. For any dynamic electrochemical system under study involving current flow, as in voltammetry, once a reaction mechanism has been postulated it is usually straightforward to write down an equivalent system of partial differential equations (when the reactive species are in solution phase), or ordinary differential equations (when the reactive species are confined to a surface) [1]. The techniques of electrochemical interrogation (voltammetry, amperometry etc) are then modelled in the boundary and initial conditions of the system. These equation systems can then be solved either analytically or (more commonly) numerically, typically to yield the current flowing in the system as a function of time or (equivalently) potential. The question then arises as to how we best use the mathematical model to estimate, from experimental data, the key parameters governing the electrochemical system under interrogation (as described above, these parameters are typically the rates of all reactions taking place, the corresponding equilibrium potentials and transfer coefficients, the double layer capacitance and any uncompensated resistance). This is known as the *inverse* problem.

Over the last 60 years, much effort has been devoted to deriving quantitative relationships between the measured outputs of voltammetric experiments and the key parameters governing those experiments in an effort to address this inverse problem. Early methods typically relied on surrogate metrics (such as the peak current in DC linear sweep voltammetry or the peak separation in DC cyclic voltammetry) that could be related algebraically to the system parameters, but such simple summary statistics are typically very susceptible to both measurement error and experimental noise [1]. Another common approach is to solve the underlying mathematical equations numerically and then heuristically adjust (or "tune") the parameters in the model (and re-solve) until a "good fit" to the experimental data is achieved (often judged by eye) [14]. As computing power has increased over the last 30 years, it has been possible to begin to consider a more automated approach to the solution of inverse problems in electrochemistry [15]. The paper by Bieniasz and Speiser [16] gives an excellent review of a wide range of parameter estimation approaches introduced into the electrochemistry literature, and itself introduces a method for assessing the statistical errors arising in parameter estimates from DC voltammetric studies. The usual approach is to set up an objective function which measures the "distance" between the experimental data (typically a time trace), and data simulated from a model that uses an initial guess for the parameters of interest. Optimisation techniques are then used to adjust (automatically) the values of the parameters to minimise this distance metric (which is usually the Euclidean or least squares distance) and yield the "best fit" to the experimental data. Whilst this optimisation approach gives (at least

for "well-posed" problems) the globally optimal solution for the parameters of interest, it generally gives only point estimates of the parameter values. Whilst these are valuable, no measure of the accuracy of the values is provided, although one can be estimated by making assumptions about the local curvature of the objective function at the optimal value [16], or by using a bootstrapping technique such as that described previously by Bieniasz and Rabitz [17] and in one of our previous papers [13]. However, the former case relies on an assumption of symmetry of the distribution of the parameters (and typically requires complex symbolic manipulation when dealing with differential equations), and the latter case (bootstrapping) is computationally very expensive (since it involves repeated solution of the full inverse problem) unless combined with approximation techniques that obviate the need to solve the underlying system of differential equations repeatedly [17].

In other fields of science, and in other areas of chemistry [18, 19, 20], an increasingly common approach is to place the inverse problem in a Bayesian framework. This then admits the use of computational approaches such as Markov Chain Monte Carlo (MCMC) methods to provide an estimate not only of the optimal parameter values but also of the likely spread of those parameters about that optimum; this is achieved by direct sampling of the joint probability distributions of the parameters and therefore requires only repeated solution of the forwards problem (albeit typically tens of thousands of times). To our knowledge, this approach of directly addressing the estimation of the distribution of the recovered parameters in voltammetric experiments using Bayesian methods has not been described previously. In an excellent tutorial paper in 2009 on the use of Bayesian methods for chemistry data, Armstrong and Hibbert [18] included an example (see sections 5.1 and 5.2) involving the use of electrochemical sensing to determine the concentration of lead in drinking water, but the parameter estimation was based on a simple algebraic hyperbolic relationship between the system parameters and the measured current, rather than the solution of an underlying system of differential equations that describes the physical processes of the whole system, as we describe here. Similarly, in the PhD thesis of Samuel [21], Bayesian methods are used to recover distributions of surrogate metrics (such as the peak and minimum current) derived from voltammetric data analysing the effects of levels of carbon on the electrical output of battery power sources. The Bayesian approach of parameter estimation using Gaussian Process regression to estimate parameter values in voltammetric experiments has also been described [22, 23], but again these do not allow direct sampling of the posterior distributions of the parameters of interest. For a more comprehensive review of the use of Bayesian approaches in chemistry see [18].

In this paper, we therefore address the *direct sampling* of the posterior distribution of the parameters of interest by use of Bayesian approaches. As we will show, our approach will allow us to quantify the effects of random experimental noise on the values of the recovered parameters. Bayesian inference also comes equipped with several decades of theoretical underpinning that allows related problems such as model selection (i.e. which of two or more competing models best fits the experimental data) and optimal experimental design (e.g. what is the best input signal to give the optimal amount of information about a parameter set of interest) to be addressed. This approach is therefore ideal when attempting to assess the relative information content contained within two signals arising from different experimental interrogations of the same system, as in the case of comparing DC and AC voltammetry that is our primary interest here.

In this paper we therefore give an outline of the background theory to the use of the Bayesian methods in electrode kinetics. We will illustrate the power of the method by comparing the information content of the current-potental (time) data in the case of DC and AC voltammetry at a planar electrode for the simplest case of a quasi-reversible

one-electron reaction mechanism of Eq.1. The power of the Bayesian approach becomes immediately obvious from this comparison since we are able to show that AC voltammetry is less affected by purely random experimental noise, so that in effect it has a greater information content then the corresponding DC measurement, and hence yields more accurate estimates of the experimental parameters. We also show that the AC approach can therefore yield accurate estimates across a wider range of experimental parameters, and in particular can distinguish higher values of the rate constant k_0. The results of using a MCMC approach to solving the inverse problem are given for both synthetic data (i.e. simulated data for which the true parameter values are known and to which realistic levels of simulated experimental noise have been added), and for an illustrative case of experimental data for the one-electron reduction of $[Fe(CN)_6]^{3-}$ to $[Fe(CN)_6]^{4-}$ [13]. By using synthetic data, we are also able to quantify (for the first time) the improvements in accuracy in parameter estimation resulting from using the technique of AC compared to DC voltammetry in the presence of purely random (in this case, Gaussian) experimental noise.

2 Experimental methods

Details of the single experimental data set used in this paper has been described previously in [9, 13]. In summary, this electrochemical experiment was performed in standard three-electrode cell, using a glassy carbon disk as the working electrode, and all potentials are reported versus an Ag/AgCl reference electrode. The surface area of the electrode was estimated as 0.070 cm^2 from the Randles-Sevcik relationship and data obtained by measuring DC voltammograms for oxidation of ferrocene at a known concentration in acetonitrile 0.1M(n-Bu)$_4$NPF$_6$ electrolyte. The value of the diffusion coefficient, D, of $[Fe(CN)_6]^{3-/4-}$was initially determined to be 7.2×10^{-6} cm^2s^{-1}, by analysis of the semi-integrals of background corrected DC cyclic voltammograms, taking into account edge diffusion effect, and then confirmed by simulations of cyclic voltammetric data. In this paper we make use of data set 1 in reference [13] for the reduction of aqueous 1 mM $[Fe(CN)_6]^{3-}$ in 3M KCl electrolyte.

3 Theory

3.1 Modelling

Throughout this paper, we consider only the single electron transfer process given by Eq. 1, which is the simplest possible example of an electrochemical reaction, and is the process governing our chosen experimental system. The mathematical model for this reaction mechanism is given below. Here we assume that both convection and migration can be neglected by virtue of using a macrodisk stationary electrode, and an excess of supporting electrolyte respectively. We assume equal diffusion coefficients for each species A and B ($D_A = D_B = D$) and so need to solve for the concentration of only one of the species (since the concentrations c_A, c_B of species A and B respectively, satisfy $c_A = c_\infty - c_B$, where c_∞ is the bulk concentration of species A) and we choose to solve for species A. Then by Fick's second law we obtain the equation

$$\frac{\partial c_A}{\partial t} = D\frac{\partial^2 c_A}{\partial x^2}, \tag{5}$$

where x is distance from the electrode surface and t is time. The initial and boundary conditions are

$$\begin{aligned} c_A(x,0) &= c_\infty \\ c_A &\to c_\infty, \quad \text{as} \quad x \to \infty, \quad t > 0. \end{aligned} \tag{6}$$

At the electrode surface, $x = 0$, for $t > 0$, we have the conservation and flux conditions

$$D\frac{\partial c_A}{\partial x} = \frac{I_f}{FS}, \tag{7}$$

along with the Butler-Volmer condition

$$D\frac{\partial c_A}{\partial x} = k_0 \left[c_A \exp\left((1-\alpha)\frac{F}{RT}(E_{\text{eff}}(t) - E_0)\right) - (1-c_A)\exp\left(-\alpha\frac{F}{RT}(E_{\text{eff}}(t) - E_0)\right)\right]. \tag{8}$$

Here, I_f is the faradaic current, S is the electrode area, and $E_{\text{eff}}(t)$ is the *effective* applied potential (defined below).

To complete the model, we need to define the potential to be applied at the electrode surface ($x = 0$). If we define $E_{\text{app}}(t)$ to be the applied potential, then for the case of a DC linear ramp we have

$$E_{\text{app}}(t) = E_{\text{start}} + vt, \quad 0 \le t \le t_{\max}$$

and for AC voltammetry we have

$$E_{\text{app}}(t) = E_{\text{start}} + vt + \Delta E \sin(\omega t) \tag{9}$$

where v is the sweep rate, E_{start} is the initial potential, $t_{\max}$ is the end time of the experiment, and for the AC case, ω is the radial frequency and ΔE the amplitude of the sine wave. The *effective* applied potential can now be defined as

$$E_{\text{eff}}(t) = E_{\text{app}}(t) - E_{\text{drop}} = E_{\text{app}}(t) - I_{\text{tot}}R_u$$

where E_{drop} models the effect of uncompensated resistance, R_u. I_{tot} is the total (measured) current, and combines the faradaic current and the background capacitive current, I_c, which can be modelled as

$$I_c = C_{dl}\frac{dE_{\text{eff}}}{dt}, \tag{10}$$

where C_{dl} is the double layer capacitance (assumed constant in this work), and then

$$I_{\text{tot}} = I_f + I_c. \tag{11}$$

As described in the introduction in Eqs. 4, for the case of DC voltammetric methods the values of k_0, D and v determine whether the reaction is fully-reversible (large Λ), quasi-reversible (intermediate Λ), or irreversible (small Λ).

Equations 5–11 are non-dimensionalised as described in the supplementary information. The resulting non-dimensional system of equations is solved using an implicit finite difference method with an exponentially expanding grid (as we have described in full detail previously - see [14]). Having derived the governing partial differential equations and boundary conditions for this simplest problem of the reaction mechanism in Eq. 1 we can see mathematically that the mechanism is governed by five parameters $(\tilde{k}_0, \tilde{E}_0, \tilde{\alpha}, \tilde{R}_u, \tilde{C}_{dl})$, and we will collectively denote these parameters by the vector $\boldsymbol{\theta}$. The *inverse* problem that we wish to solve can be defined as finding the best possible approximation to $\boldsymbol{\theta}$ given our measured experimental output trace of the current $I_{\text{tot}}^{\text{data}}$, versus potential, together with an estimate of the effect of experimental noise. This will be achieved by recovering the marginal posterior distributions of each parameter that are induced by the experimental noise.

Since this paper addresses the issue of the relative information content of DC and AC forms of voltammetry and therefore of the relative ability of these two forms of voltammetry to address the inverse problem, in Figure 1 we remind the reader of the way in which each of these four parameters influences the measured current in the DC case (changes in $\tilde{E}_0$ simply shift the signal to the left or right and so are not included). The similarity in the effects of some of these parameters is clear, and that differing combinations of parameters can have similar effects on the overall current should also be clear (we would highlight, in particular, that changes in both $\tilde{\alpha}$, and $\tilde{R}_u$ can be seen to be correlated with changes in $\tilde{k}_0$, i.e. the effect of decreasing $\tilde{k}_0$ will be similar to the effect of increasing $\tilde{R}_u$ and $\tilde{\alpha}$ by some suitable amount). The equivalent figure for AC voltammetry using a small amplitude signal is included in the supplementary information (see Figure S1).

In the Supplementary Information of a previous paper [13] we derived this inverse problem in the least squares sense. The process described in [13] involved making some initial guess, $\boldsymbol{\theta}_0$ say, of the five parameters of interest, and then using these to generate a simulated output trace, $I_{\text{tot}}^{\text{model}}$, by solving our system of Equations 5–11 above. We then compare how far apart the measured and simulated traces are by taking the least squares difference between them. Assuming that we have T data points, and we solve for the simulated current at the same T points, the least squares difference is calculated as

$$O_{LS} = \sum_{t=1}^{T} \left(I_{\text{tot,t}}^{\text{data}} - I_{\text{tot},t}^{\text{model}} \right)^2, \tag{12}$$

where O_{LS} is usually termed the least squares *objective function*. The inverse problem is then to find the value of the parameters $\boldsymbol{\theta}_0$ that minimises this objective function. This is an optimisation problem and there is available a wide range of algorithms and software to solve this type of problem (in our previous work we used a Quasi-Newton method that is available within the NAG Library [24]).

3.2 Parameter Inference

In describing our approach to the parameter recovery problem we will follow the Bayesian Inference approach that we have described previously in a paper related to an application in cardiac cell biology [19]. To aid our description, we first introduce some simpler notation. We denote by $\mathbf{y} = (y_1, \ldots, y_T)$ our experimental data trace, that is, the total measured current $I_{\text{tot, t}}^{\text{data}}$ at each time point. Throughout, we assume that all experimental measurements are subject to normally distributed random noise with mean zero and standard deviation σ, and that this is the only source of error in our data. In a previous

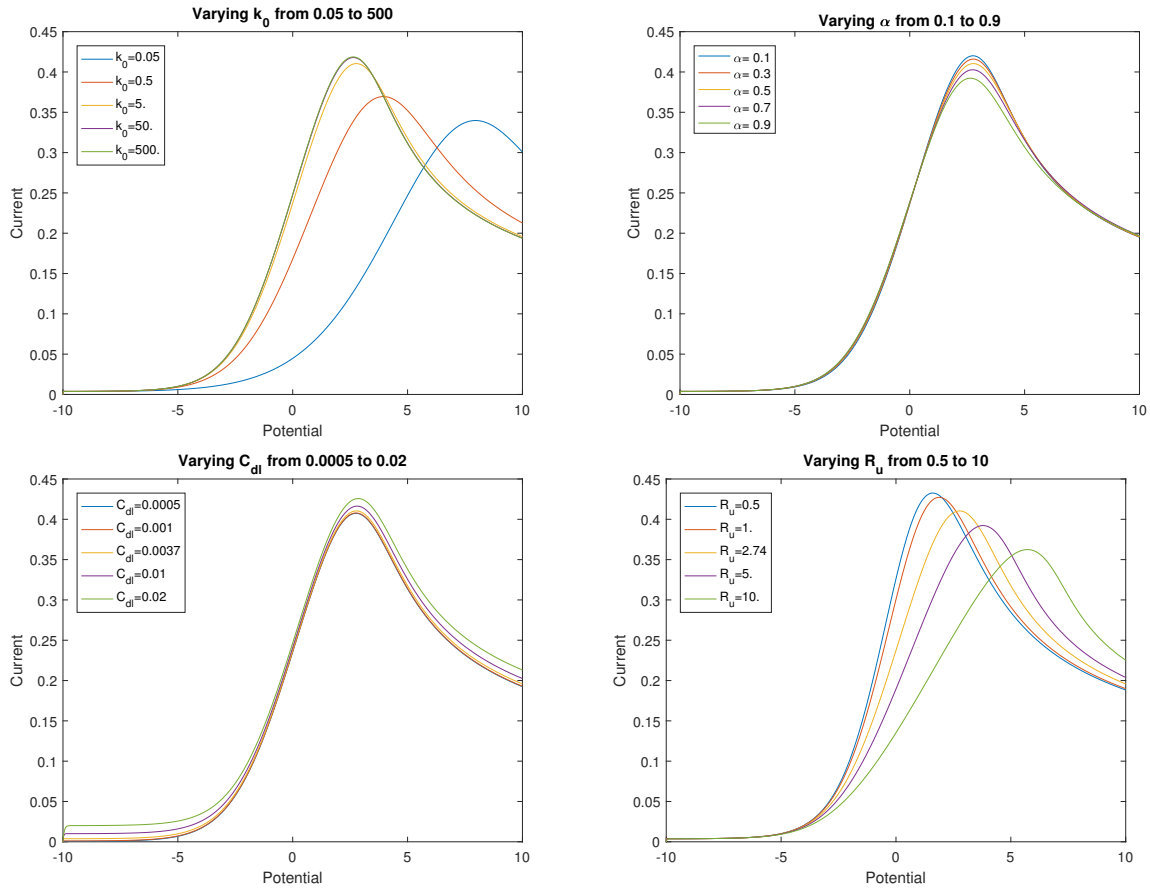

Figure 1: Plots that show the effect of changing the designated parameters in simulated currents obtained as a function of potential from numerical solution of the model equations in response to a linear sweep of the DC potential. All non-dimensional parameters take the values $\tilde{k}_0 = 5$, $\tilde{\alpha} = 0.5$, $\tilde{E}_0 = 0$, $\tilde{C}_{dl} = 0.0037$, and $\tilde{R}_u = 2.74$, unless indicated otherwise. Assuming values of the diffusion coefficient of $D = 2 \times 10^{-5}$ cm^2 s^{-1}, electrode area $S = 1$ cm^2, sweep rate $v = 1$ V s^{-1}, and $c_\infty = 1$ mM at a temperature of 298 K, these values correspond to dimensional values of $R_u = 26.15$ Ω, $C_{dl} = 10^{-5}$ F, and $k_0 = 0.140$ cm s^{-1}.

paper (see Figure 4 and Table S2 of [13]) we demonstrated through analysis of experimental data, that this is a reasonable assumption, and that typical values of the standard deviation of the experimental noise are in the range 1% to 2% of the peak current.

3.3 Bayes' rule

We have assumed in developing our model of the underlying electrochemical system captured in Equations 5 to 11 above that the observed experimental data $\mathbf{y}$ is a function of the parameters of interest $\boldsymbol{\theta}$. We now make the further assumption that the parameters $\boldsymbol{\theta}$ are themselves drawn from a probability distribution, and we frame our inverse problem as trying to find that probability distribution for $\boldsymbol{\theta}$ *given the observed values of the data* $\mathbf{y}$. We denote this probability distribution as $P(\boldsymbol{\theta}|\mathbf{y})$, with the vertical line indicating that the values of $\mathbf{y}$ are *given*. In Bayesian inference, the distribution $P(\boldsymbol{\theta}|\mathbf{y})$ is termed the *posterior probability density* or *posterior distribution*, since it is the inferred distribution of $\boldsymbol{\theta}$ as a result of having observed the data $\mathbf{y}$, and it is this distribution that we want to approximate.

With these definitions in place we, we can now make use of Bayes' rule which states

$$P(\boldsymbol{\theta}|\mathbf{y}) = \frac{P(\mathbf{y}|\boldsymbol{\theta})P(\boldsymbol{\theta})}{P(\mathbf{y})}. \tag{13}$$

In Equation (13), $P(\boldsymbol{\theta})$ is called the prior distribution of $\boldsymbol{\theta}$ and is chosen to give the best representation of any prior beliefs or knowledge that we have before observing any experimental data about the distribution of $\boldsymbol{\theta}$.

The distribution $P(\mathbf{y}|\boldsymbol{\theta})$ is the probability density of the experimental data $\mathbf{y}$ given a model parameterized with parameters $\boldsymbol{\theta}$, and is termed the *likelihood* of the data given this particular set of parameters $\boldsymbol{\theta}$; assuming that we know the distribution of the errors in the data then this likelihood can be calculated, as described below. $P(\mathbf{y})$ is a normalizing term (which is the integral of all possible densities $P(\mathbf{y}, \boldsymbol{\theta}) = P(\mathbf{y}|\boldsymbol{\theta})P(\boldsymbol{\theta})$ over all values of $\boldsymbol{\theta}$)), and ensures that the posterior density $P(\boldsymbol{\theta}|\mathbf{y})$ integrates to 1. In practice, the calculation of this normalising term (which can be very computationally expensive) is avoided by considering ratios of the likelihood.

3.4 Calculating the prior

In most experimental situations in electrochemistry, *a priori* we will have only a rough idea of what the values of the parameters are likely to be. In this situation it is usual to assume that the possible values of the parameters are distributed uniformly across suitably chosen intervals large enough that they are known to contain the true parameter value (that is we are choosing an "uninformative" prior). Their joint prior distribution is then given by

$$P(\boldsymbol{\theta}) = \begin{cases} c, \ \{\boldsymbol{\theta}\} \text{ in some suitably chosen 5-dimensional hypercube,} \\ 0, \ \text{otherwise,} \end{cases} \tag{14}$$

where c is a non-zero finite normalizing constant. In practice, this simply means that we place sensible physical bounds on our possible choices of the five parameter values to be investigated. For example, $\tilde{\alpha}$ is limited to the range $0 < \tilde{\alpha} < 1$.

3.5 Calculating the likelihood

As noted earlier, we have previously shown the experimental error present in the data from our voltammetric studies to be normally distributed [13], with zero mean and standard deviation on the order of $1-2\%$ of the peak current. Rather than assuming a particular value for the standard deviation, σ, of the noise, we can also incorporate it into our inference problem. Writing the likelihood as

$$L(\boldsymbol{\theta}|\mathbf{y}) = P(\mathbf{y}|\boldsymbol{\theta}), \tag{15}$$

then Bayes' rule (in Equation (13)) can be rewritten in terms of the likelihood as

$$P(\boldsymbol{\theta}|\mathbf{y}) \propto P(\boldsymbol{\theta})L(\boldsymbol{\theta}|\mathbf{y}). \tag{16}$$

When the prior distribution is assumed to be uniform (as in this study), then we can make inferences based on just the likelihood, as the prior $P(\boldsymbol{\theta})$ is either constant or zero.

Since we assume that the errors at each time point are independent, the conditional probability density of observing the whole experimental trace from time sample 1 to time sample T given the model parameter set $\boldsymbol{\theta}$ is simply the product of the probability density functions at each time point

$$L(\boldsymbol{\theta}|\mathbf{y}) = \prod_{t=1}^{T} P(y_t|\boldsymbol{\theta}). \tag{17}$$

With our further assumption that the experimental noise is also normally distributed with a mean of zero and variance of σ^2, the likelihood can be expressed as

$$L(\boldsymbol{\theta}|\mathbf{y}) = \prod_{t=1}^{T} \mathcal{N}(y_t|f_t(\boldsymbol{\theta}), \sigma^2) = \prod_{t=0}^{T} \frac{1}{\sqrt{2\pi\sigma^2}} \exp\left(-\frac{\left(y_t - f_t(\boldsymbol{\theta})\right)^2}{2\sigma^2}\right), \tag{18}$$

where for notational simplicity we have set $f_t(\boldsymbol{\theta}) = I_{\mathrm{tot},t}^{\mathrm{model}}$. Since we do not in practice know the value of σ^2, the standard deviation of the experimental noise, we will also find this additional parameter value as part of the inverse problem (i.e. we actually estimate six parameters in total).

3.6 Generating synthetic data

In our case $f_t(\boldsymbol{\theta})$ is the predicted current at each time point given a particular set of parameter values, which is calculated by solving Equations 5 to 11. For most of the results contained in this paper we will make use of "synthetic" experimental data, i.e. we will generate experimental data sets by solving Equations 5 to 11 for a chosen set of values of $\boldsymbol{\theta}$, and then we will add randomly generated Gaussian noise at each point with mean zero and standard deviation proportional to the maximum current (typically we will choose a standard deviation in the range 0.5% to 2% of the peak current value).

3.7 Maximising the likelihood

Finding the values of the parameters that maximise the likelihood is a classical statistical method for determining point estimates of parameters. As we described in the earlier literature review, under certain conditions, we can assume asymptotic normality of these maximum likelihood estimators and the Fisher Information matrix can be shown to approximate the covariance matrix of the asymptotic distribution of the maximum likelihood

estimator [25], hence allowing us to to obtain confidence intervals for the parameter estimates. However, this approach has two major disadvantages. Firstly, it requires that we can diffferentiate the likelihood with respect to the parameters; in most cases in electrochemistry where the underlying model is a system of ordinary or partial differential equations this is complex and will require the use of automated algebraic manipulation software, and the calculation will need to be repeated for every possible reaction mechanism. Secondly, this approach assumes that the distributions of the parameter values are symmetric but we know for the model under consideration here, for example, that the distribution of $\tilde{k}_0$ will be asymmetric for large enough values of $\tilde{k}_0$. Instead in this paper we utilise the Bayesian approach to obtaining the posterior distribution $P(\boldsymbol{\theta}|\mathbf{y})$ via the MCMC approach.

3.7.1 Markov Chain Monte Carlo parameter inference

To obtain a sample from the posterior distribution $P(\boldsymbol{\theta}|\mathbf{y})$ we choose to use an efficient method based on the well-known Metropolis-Hastings algorithm [26]. Comprehensive descriptions of the theory of MCMC can be found in the statistics literature (see for example [27]). However, since this is the first time (to our knowledge) that MCMC methods have been described in the electrochemistry literature for the estimation of electrode kinetic parameters in voltammetry, we give a brief outline of how the method works here.

Our aim is to find an approximation to the posterior distribution $P(\boldsymbol{\theta}|\mathbf{y})$ by drawing a finite (but sufficiently large to be accurate) sample from this distribution. To do this we simulate a Markov Chain whose limiting distribution (as the sample size increases) is the required posterior distribution using the well-known *Metropolis-Hastings* algorithm [26]. In this algorithm, candidate parameter sets are proposed from a *proposal distribution* $q(\boldsymbol{\theta_{cand}}|\boldsymbol{\theta_i})$ which depends only on the previously accepted parameter set $\boldsymbol{\theta_i}$. Throughout this paper we will use a multivariate normal distribution as our proposal distribution. Any candidate parameter set $\boldsymbol{\theta_{cand}}$ is then compared to the current parameter set $\boldsymbol{\theta_i}$ by calculating the ratio of the posterior of the two parameter sets, and the value of the ratio determines whether or not the proposed parameter set is accepted as part of the MCMC chain.

If the candidate parameter set has a greater posterior density value than the existing parameter set then it will be added to the Markov chain, that is $\boldsymbol{\theta_{i+1}} = \boldsymbol{\theta_{cand}}$. Otherwise, the parameter set is accepted with a probability equal to the ratio of posterior density values which can be evaluated using Eq. 16. If the proposed parameter set contains any parameters outside the range of the prior, or violates any of the conditions on the parameters that we have imposed, the parameter set is assigned an acceptance probability of 0, i.e. it is immediately rejected, and the previously accepted parameter set is added to the Markov chain — that is, $\boldsymbol{\theta_{i+1}} = \boldsymbol{\theta_i}$. Otherwise, (making use of Eq. 16) a proposed parameter set generated from a multivariate normal distribution is accepted with probability, r, given by

$$r = \min\left\{\frac{L(\boldsymbol{\theta_{cand}}|\mathbf{y})}{L(\boldsymbol{\theta_i}|\mathbf{y})}, 1\right\}. \tag{19}$$

In the above equation, we have cancelled the prior distribution since it is constant on parameters that are within range (see Eq. 14). If the proposed parameter set is rejected (with probability $1-r$), then the previously accepted parameter set is again added to the Markov chain — that is, $\boldsymbol{\theta_{i+1}} = \boldsymbol{\theta_i}$.

Since the likelihoods for large samples are extremely small, in practice we work with the

natural log of the likelihood (which is a monotonic increasing function and is maximised by the same value of $\boldsymbol{\theta}$ as the likelihood), giving:

$$\begin{aligned} l(\boldsymbol{\theta}|\mathbf{y}) &= \log(L(\boldsymbol{\theta}|\mathbf{y})) \\ &= -\frac{T}{2}\log(2\pi\sigma^2) - \frac{1}{2\sigma^2}\sum_{t=1}^{T}(y_t - f_t(\boldsymbol{\theta}))^2 \\ &= -\frac{T}{2}\log(2\pi) - T\log(\sigma) - \frac{1}{2\sigma^2}\sum_{t=1}^{T}(y_t - f_t(\boldsymbol{\theta}))^2 \end{aligned} \tag{20}$$

Since the first term on the RHS of Equation (20) is constant for all proposed $\boldsymbol{\theta}$, it will cancel with itself when we take differences of log-likelihoods in the Metropolis-Hastings algorithm. We therefore define the simpler log-likelihood as

$$l(\boldsymbol{\theta}|\mathbf{y}) = -T\log(\sigma) - \frac{1}{2\sigma^2}\sum_{t=1}^{T}(y_t - f_t(\boldsymbol{\theta}))^2, \tag{21}$$

and this is the quantity that is calculated in the algorithm given in the supplementary information (note that we retain the terms in σ since this parameter will also be estimated as part of the inference problem). In that algorithm, we use a covariance matrix adaptive version of the Metropolis-Hastings Algorithm which helps identify the directions in parameter space which have the highest likelihood values, the algorithm is described in [28]. At each iteration of the algorithm, the covariance matrix of the multivariate normal distribution is updated and a scalar value is also updated to define the width of the distribution. In the results presented in this paper, we run our MCMC chains for 40,000 samples and discard the first 10,000 samples as 'burn in' (for an introduction to MCMC see [27]). To ensure efficiency in our Monte-Carlo sampling, we first find the location of the optimum using a standard global minimisation algorithm (we use both the *fminsearch* algorithm and the *cma-es* algorithms that are available in the Matlab [29] software package), which we use as a seed point for the MCMC algorithm as described in the supplementary information.

In the results section, these samples are shown as histograms which illustrate the nature of the posterior distribution.

4 Results

To illustrate the advantages of taking a Bayesian approach we first consider its use in recovering the parameter values of interest from a standard DC linear sweep voltammetry experiment. We show that by recovering the posterior distribution we have a direct means of assessing both the accuracy with which each parameter can be recovered from the data in the presence of known levels of (initially synthetic) noise, and the impact of increasing levels of experimental noise on that accuracy. This then gives us a direct means of comparing the information content of standard DC linear sweep voltammetry and AC voltammetry.

4.1 Bayesian inference in DC linear sweep voltammetry

In the left hand panel of Figure 2 we show the simulated current obtained by solving Equations 5–11 for the case of linear sweep voltammetry (i.e. in the absence of a sinusoidal

oscillation). We choose to set the non-dimensional parameters $\tilde{k}_0 = 5$, $\tilde{E}_0 = 0$, $\tilde{\alpha} = 0.5$, $\tilde{R}_u = 2.74$, and $\tilde{C}_{dl} = 0.0037$ (with standard values of other parameters, e.g. $D = 2\times10^{-5}$ cm^2 s^{-1}, $S = 1$ cm^2, $c_\infty = 1$ mM, and $v = 0.1$ V s^{-1}, this equates to dimensional values of $k_0 \approx 0.14$ s^{-1}, $R \approx 25$ Ω, $C_{dl} \approx 10$ μF cm^{-2}) so that we are in the middle of the quasi-reversible region and so it should be possible to recover all parameters from the data set. The red curve gives the simulated current and the blue curve shows the same simulated current but with added Gaussian noise with mean zero and standard deviation equivalent to 0.5% of the maximum value of the current [1].

Figure 3 shows the results of using this simulated noisy data trace (i.e. the blue curve in the left panel of Figure 2) in our MCMC parameter recovery algorithm. The diagonal of the figure gives the plots of the posterior distributions for each of the five parameters contained in $\boldsymbol{\theta} = (\tilde{k}_0, \tilde{\alpha}, \tilde{C}_{dl}, \tilde{R}_u, \tilde{E}_0)$ (we omit the plots of the recovered distribution of the standard deviation, σ). Each of these distributions can be seen to be symmetric and appear approximately Gaussian in shape. On the sub-diagonals of the figure we give "biplots" of each of the pairs of variables - these allow us to observe whether there are any significant correlations between pairs of parameters.

In the third row of Table 1, we give the mean values of the recovered parameters from these posterior distributions (calculated as the mean of the samples shown on the diagonals in Figure 3), together with their standard deviations to give some measure of accuracy. As can be seen the values recovered are close to the true values used in generating the simulated trace. In Figure 4 and Table 1 we illustrate the effect of varying the amount of experimental noise by reducing the standard deviation of the simulated experimental noise from 2% of the maximum value of the current, to 1% and then to 0.5%. As can be seen, the width of the recovered posterior distributions decreases as expected, with the standard deviation of the recovered distribution for $\tilde{k}_0$, for example, decreasing from approximately 22% of the true value, to 13% to 6% i.e. it roughly halves as the magnitude of the experimental noise halves. **The random shift in the mean of the recovered distributions is due to using different realisations of the noise term in each simulation (as explained further below), but in all cases the true underlying value of the parameters is covered by the recovered distribution (as expected).**

5 Comparison with AC Voltammetry

In this section we give similar results to the DC case but this time using an input signal with a large amplitude sine wave oscillation added to the linear DC ramp, as illustrated in the right hand panel of Figure 2. The illustrative case that we choose uses a value of the sine wave frequency of non-dimensional $\tilde{\omega} = 16\pi$ in Equation (9), and an amplitude $\Delta\tilde{E}$ of 4.0 (in dimensional units assuming a sweep rate of 0.1 V s^{-1}, this corresponds to a frequency of around 15Hz and an amplitude of about 150 mV - that is a relatively high frequency and a large amplitude). The optimal choice of AC parameter values is discussed

[1] **It is worth noting that we have solved Equations 5–11 numerically which introduces a second level of error into the solutions. However, based on our previous work [14] we have chosen numerical parameters - the space and time steps - sufficiently small that these numerical errors are negligible compared to the Gaussian noise that is added to the simulated signal. We have also assumed the the experimentally measured and recorded timesteps (i.e. the times at which the current is recorded) are measured accurately so that there is a perfect match between the timesteps used in the simulation and the measured timesteps from the experiment.**

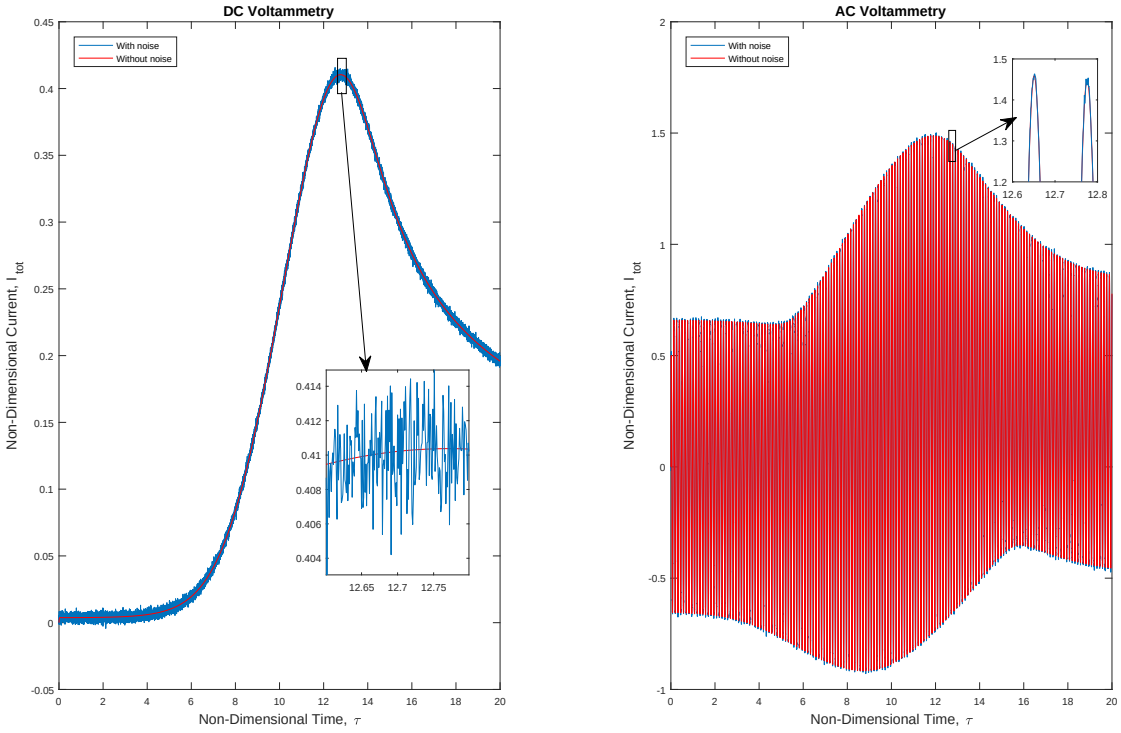

Figure 2: Current-potential traces obtained by solving 5–11 with non-dimensional parameters $\tilde{k}_0 = 5$, $\tilde{E}_0 = 0$, $\tilde{\alpha} = 0.5$, $\tilde{R}_u = 2.74$, and $\tilde{C}_{dl} = 0.0037$ (with standard values of other parameters, e.g. $D = 2 \times 10^{-5}$ cm^2 s^{-1}, $A = 1$ cm^2, $c_\infty = 1$ mM, and $v = 0.1$ V s^{-1}, this equates to dimensional values of $k_0 \approx 0.14$ s^{-1}, $R \approx 25$ Ω, $C_{dl} \approx 10$ μF cm^{-2}). The left panel shows the case for DC linear sweep voltammetry, and the right trace shows the case of AC voltammetry where a sinusoidal oscillation with non-dimensional amplitude $\Delta\tilde{E} = 4.0$ and frequency $\tilde{\omega} = 16\pi$ (corresponding to dimensional values of approximately 150mV and 15 Hz) has been added to the linear ramp. In both cases, the solid red curve shows the noise-free curve, whilst the the blue curve shows the same simulated current but with added Gaussian noise with mean zero and standard deviation equivalent to 0.5% of the maximum value of the current. Note that the red and blue traces are effectively indistinguishable at the selected resolution for the AC case.

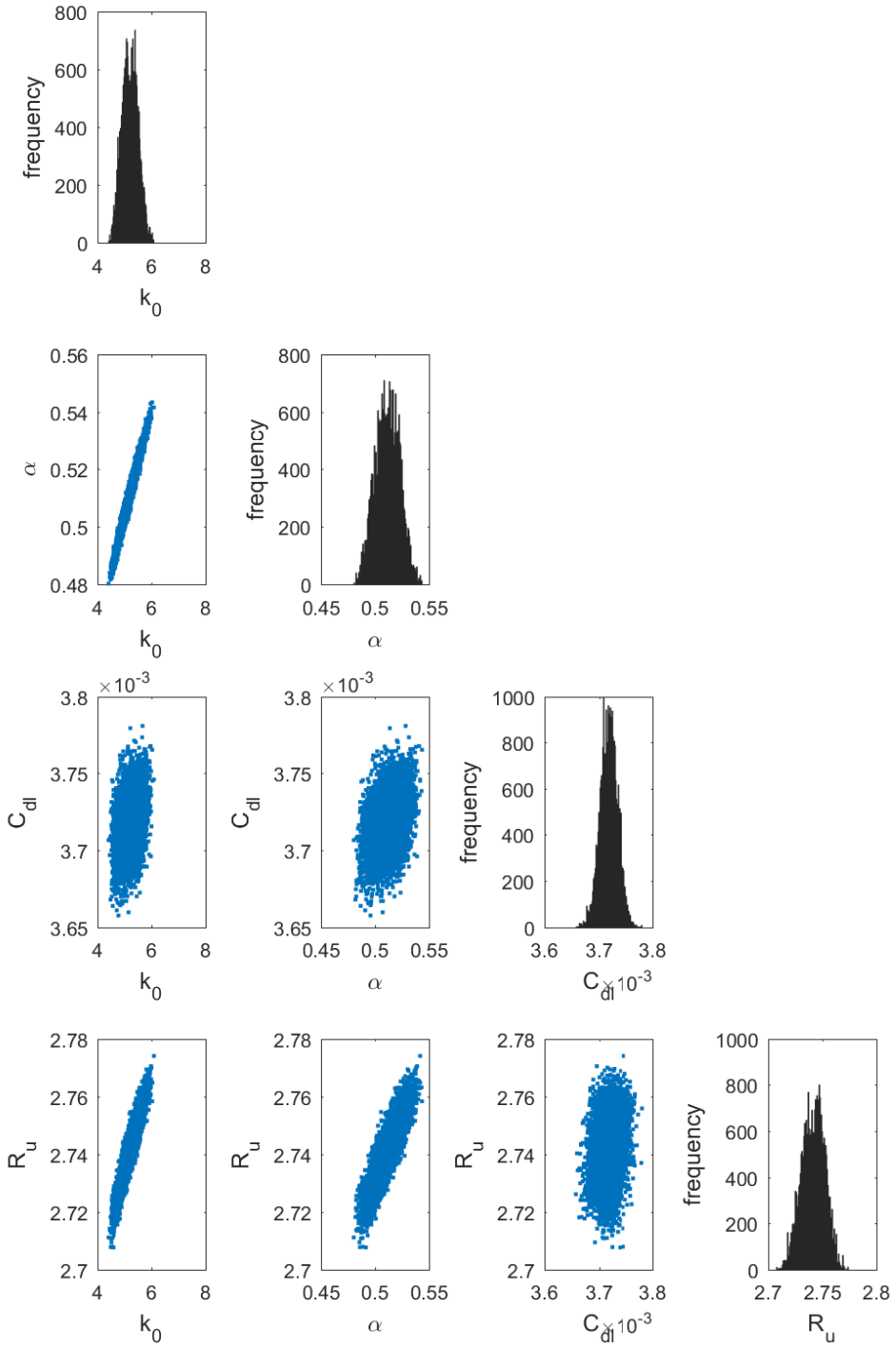

Figure 3: The results of the parameter recovery process for the DC case. On the diagonal are shown the posterior distributions for each of the five parameters of interest. On the sub-diagonals of the figure we give biplots of each of the pairs of variables. The default non-dimensional values of $\tilde{k}_0 = 5$, $\tilde{\alpha} = 0.5$, $\tilde{E}_0 = 0$, $\tilde{R}_u = 2.74$ and $\tilde{C}_{dl} = 0.0037$ were used to generate the synthetic data.

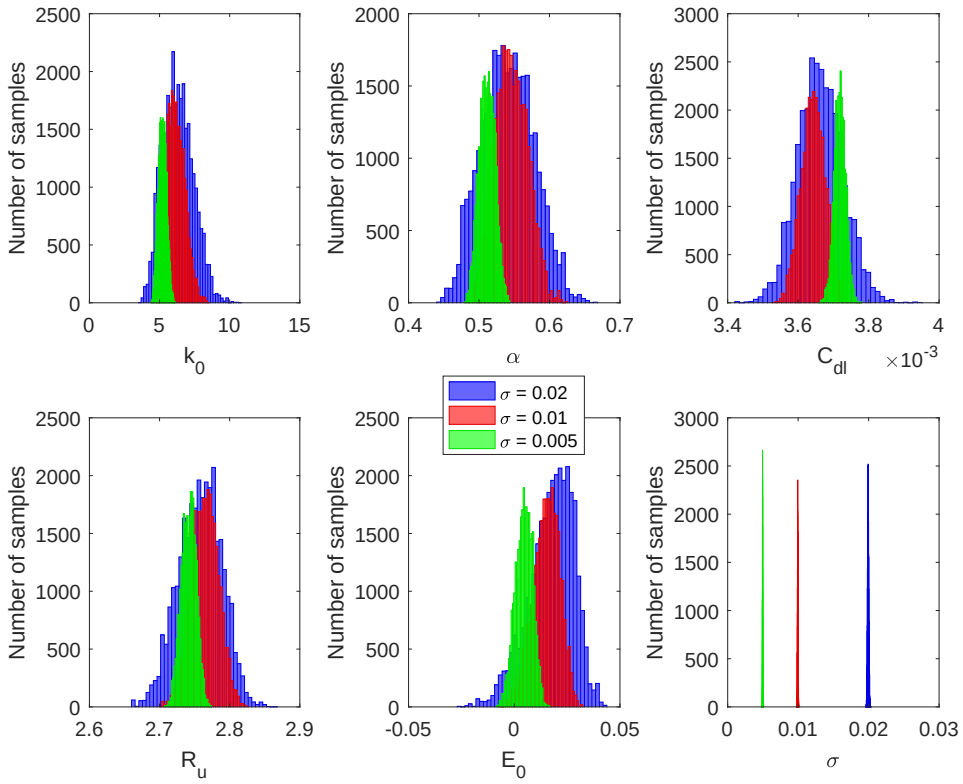

Figure 4: The effect of reducing the amount of experimental noise on the DC signal from 2% of the maximum value of the current, to 1% and then to 0.5%. The default non-dimensional values of $\tilde{k}_0 = 5$, $\tilde{\alpha} = 0.5$, $\tilde{E}_0 = 0$, $\tilde{R}_u = 2.74$ and $\tilde{C}_{dl} = 0.0037$ were used to generate the synthetic data.

Noise %	$\tilde{k}_0$ (s.d.)	$\tilde{\alpha}$ (s.d.)	$\tilde{C}_{dl}$ (s.d.) ($\times 10^3$)	$\tilde{R}_u$ (s.d.)	$\tilde{E}_0$ (s.d.)	σ
2	6.32 (1.08)	0.541 (0.037)	3.663 (0.064)	2.758 (0.031)	0.0176 (0.0105)	0.0199
1	6.13 (0.67)	0.546 (0.023)	3.643 (0.034)	2.764 (0.019)	0.0151 (0.0063)	0.0099
0.5	5.21 (0.30)	0.511 (0.011)	3.718 (0.016)	2.741 (0.010)	0.0046 (0.0040)	0.0050

Table 1: The mean values of the recovered parameters from the posterior distributions together with their standard deviations (in brackets) for the DC case as the amount of experimental noise is reduced from 2% of the maximum value of the current, to 1% and then to 0.5%. Row 3 corresponds to the results shown in Figure 3. The default non-dimensional values of $\tilde{k}_0 = 5$, $\tilde{\alpha} = 0.5$, $\tilde{E}_0 = 0$, $\tilde{R}_u = 2.74$ and $\tilde{C}_{dl} = 0.0037$ were used to generate the synthetic data.

in the next section. We have again chosen a value of standard deviation of 0.5% of the maximum current for the experimental Gaussian noise distribution in Figure 5 (although it should be noted that this is actually a larger absolute level of noise than we used in the above DC case since the maximum current is 3 times larger in the AC case).

As can be seen in Figure 5, a similar pattern of parameter recovery is observed for the AC case, although the widths of the recovered distributions are much narrower than in the DC case. The degree of improvement in the accuracy of the recovered parameters can be seen in Figure 6 and Table 2, which give the comparable AC results to the DC results shown in Figure 4 and Table 1. Again, to choose $\tilde{k}_0$ as an example, the standard deviation of the error for the AC case is just 0.84% of the true value with noise levels at 2% of the maximum current, which drops to just 0.2% with a noise level of 0.5% of the maximum current. For all parameters, the effect of random noise on the recovered value is clearly scaling linearly. The results in Tables 1 and 2 also allow us to assess the degree to which the recovery process for each parameter is affected individually. At the lowest level of noise, from the DC signal we can recover $\tilde{k}_0$ with an standard deviation of 6% of the true value, $\tilde{\alpha}$ to 2.2% of its true value, $\tilde{C}_{dl}$ to 0.42%, and $\tilde{R}_u$ to 0.36%. The equivalent figures for the AC parameter recovery are 0.21%, 0.14%, 0.02%, and 0.02%, so that the AC approach is much less affected by realistic levels of experimental noise (by a factor of between 15 and 30 depending on the parameter).

Noise %	$\tilde{k}_0$ (s.d.)	$\tilde{\alpha}$ (s.d.)	$\tilde{C}_{dl}$ (s.d.) ($\times 10^3$)	$\tilde{R}_u$ (s.d.)	$\tilde{E}_0$ (s.d.)
2	4.851 (0.0420)	0.5085 (0.0031)	3.698 (0.0029)	2.734 (0.0028)	0.01058 (0.0026)
1	4.972 (0.0217)	0.4967 (0.0015)	3.699 (0.0014)	2.739 (0.0014)	0.00361 (0.0013)
0.5	4.960 (0.0107)	0.4999 (0.0007)	3.702 (0.0007)	2.738 (0.0007)	0.00080 (0.0007)

Table 2: The effect of reducing the amount experimental noise on the AC signal from 2% of the maximum value of the current, to 1% and then to 0.5%. Row 3 corresponds to the results shown in in Figure 5). The default non-dimensional values of $\tilde{k}_0 = 5$, $\tilde{\alpha} = 0.5$, $\tilde{E}_0 = 0$, $\tilde{R}_u = 2.74$, $\tilde{C}_{dl} = 0.0037$, $\Delta\tilde{E} = 4.0$, and $\tilde{\omega} = 16\pi$ were used to generate the synthetic data.

It should be noted that all of the above results are for single realisations of the process i.e. for each numerical experiment, we generate a single noise trace from the appropriate Gaussian distribution and then add this to the simulated trace and recover the parameters using the algorithm given in the

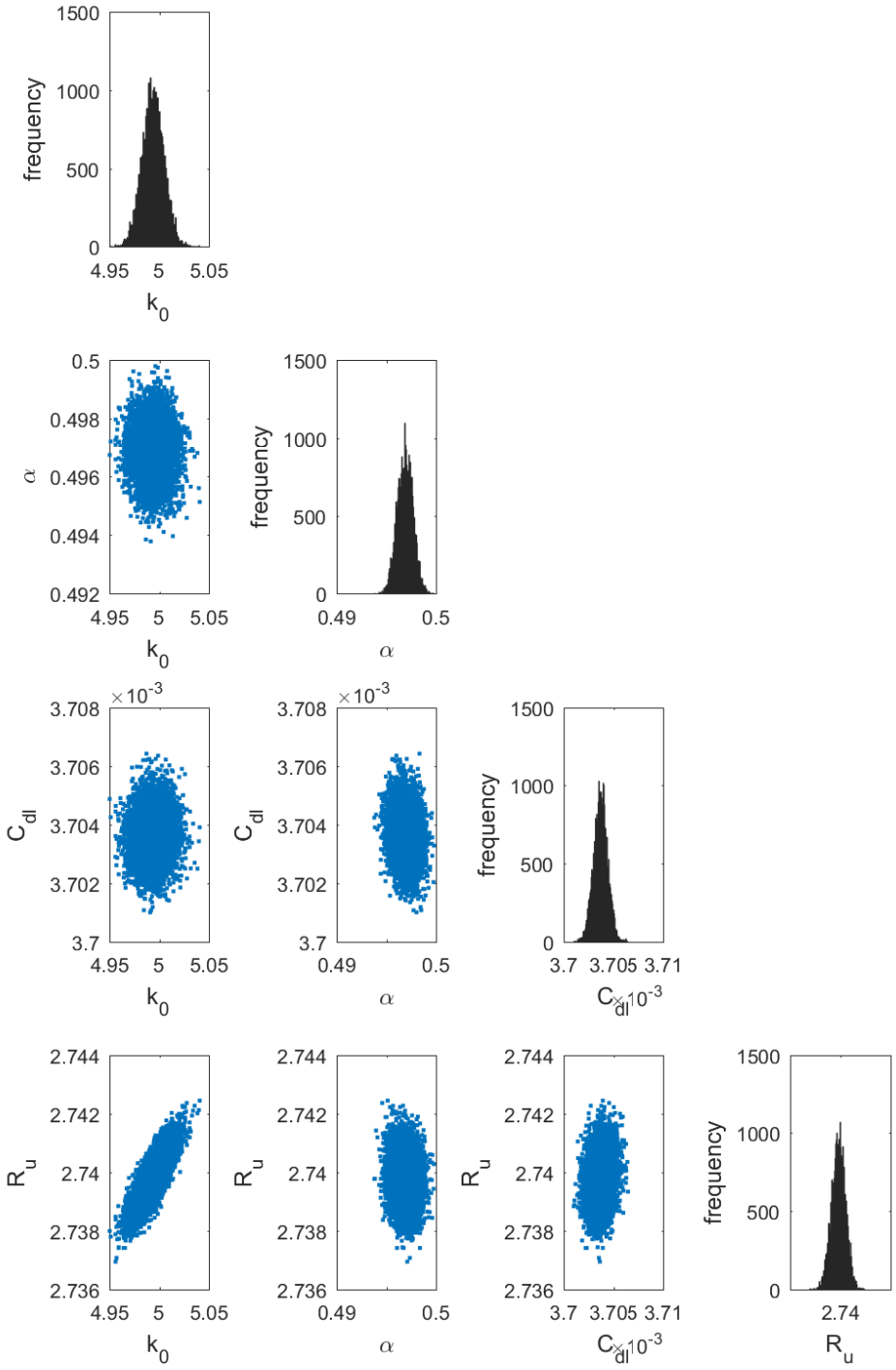

Figure 5: The results of the parameter recovery process for the AC case. On the diagonal are shown the posterior distributions for each of the five parameters of interest. On the sub-diagonals of the figure we give biplots of each of the pairs of variables.The default non-dimensional values of $\tilde{k}_0 = 5$, $\tilde{\alpha} = 0.5$, $\tilde{E}_0 = 0$, $\tilde{R}_u = 2.74$, $\tilde{C}_{dl} = 0.0037$, $\tilde{\Delta E} = 4.0$, and $\tilde{\omega} = 16\pi$ were used to generate the synthetic data.

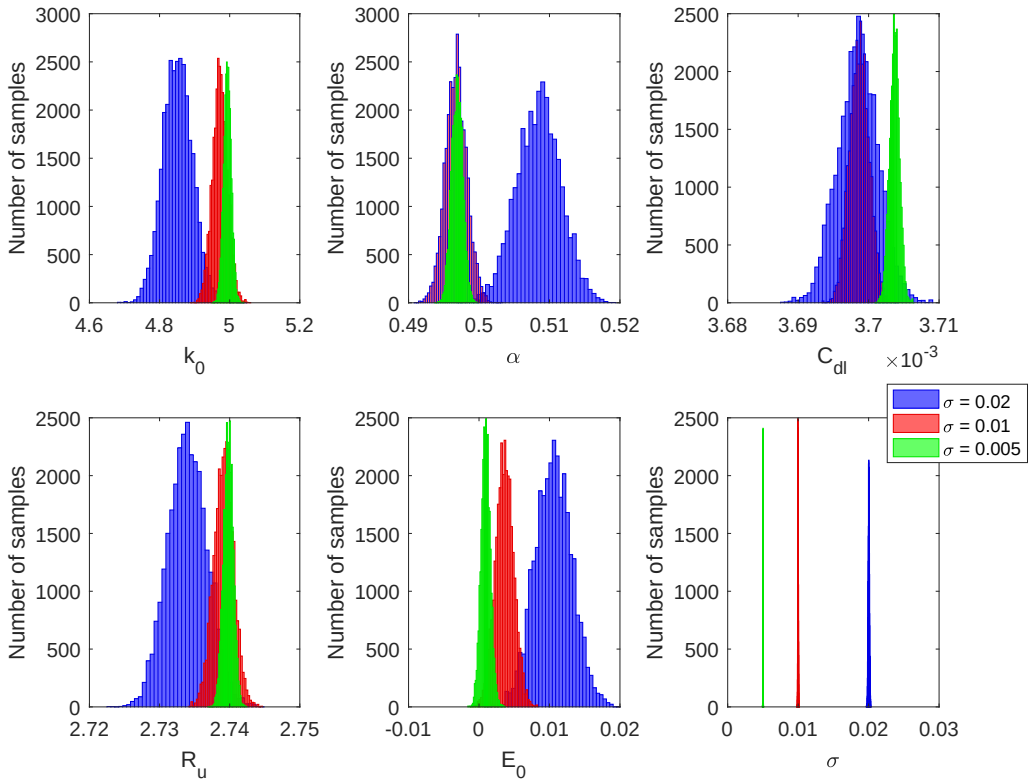

Figure 6: The mean values of the recovered parameters from the posterior distributions together with their standard deviations for the AC case as the amount of experimental noise is reduced from 2% of the maximum value of the current, to 1% and then to 0.5%. The default non-dimensional values of $\tilde{k}_0 = 5$, $\tilde{\alpha} = 0.5$, $\tilde{E}_0 = 0$, $\tilde{R}_u = 2.74$, $\tilde{C}_{dl} = 0.0037$, $\tilde{\Delta E} = 4.0$, and $\tilde{\omega} = 16\pi$ were used to generate the synthetic data.

supplementary information (note that the noise traces are different for each numerical experiment). Any single realisation may give slightly biased values of the recovered parameters or may be unduly affected by random outliers. In Table 3 we give the results of 3 repeated realisations of this process (i.e. we use the same underlying numerical solution of Equations 5–11, but on each occasion add a different realisation of the noise trace each drawn from a Gaussian distribution at noise level 0.5%), showing the recovered values of the mean and standard deviation of the recovered posterior distribution for each parameter. As can be seen, these show a remarkable degree of consistency across the three realisations. This consistency can be explained as follows. Each of the three simulated experimental noise traces is truly Gaussian and is added at every simulated time point. As we explain in the Supplementary Information, we ensure accuracy in the simulated solution of the partial differential equation defined in Eq. 5 by using 20000 time points. The recovery process then fits the best curve through the noisy data trace using the algorithm given in the Supplementary Information, and this process includes fitting the best fit of the noise distribution. With (in effect) 20000 samples available from this distribution, we can fit the noise very accurately, and the average effect of this noise on the other recovered parameters is relatively small.

The standard deviations on the recovered parameter values are therefore a measure only of the degree to which random experimental noise affects the recovery process and, as we have shown, with this number of data points the recovery process, at least for the AC signals, is very robust to this type of noise. In the Experimental section later in this paper, we demonstrate that the same is true for experimental data, where the sampling rate is actually even higher (i.e. we sample at even more time points). It is, however, worth noting that whilst this Bayesian approach gives us a very robust method of recovering parameters from noisy data; it does not tell us anything about any other sources of either stochastic or deterministic variability within the system. This system-level variability is typically caused by small differences in experimental conditions between repeated runs of the "same" experiment (examples include changes in the electrode surface due to polishing, slight variations in temperature, changes in concentration due to solvent evaporation or instability, variations in the potential of a reference electrode etc.), and these must be investigated separately.

$\tilde{k}_0$ (s.d.)	$\tilde{\alpha}$ (s.d.)	$\tilde{C}_{dl}$ (s.d.) ($\times 10^3$)	$\tilde{R}_u$ (s.d.)	$\tilde{E}_0$
4.993 (0.0109)	0.4969 (0.00079)	3.704 (0.00071)	2.740 (0.00069)	0.0009567 (0.000661)
4.960 (0.0107)	0.4999 (0.00078)	3.703 (0.00073)	2.738 (0.00070)	0.0008020 (0.000659)
4.994 (0.0107)	0.4971 (0.00077)	3.701 (0.00072)	2.740 (0.00069)	0.0003846 (0.000641)

Table 3: The results of 3 repeated realisations of the recovery process for the AC case using a noise level of 0.5%, showing the recovered values of the mean and standard deviation of the recovered posterior distribution for each parameter. The default non-dimensional values of $\tilde{k}_0 = 5$, $\tilde{\alpha} = 0.5$, $\tilde{E}_0 = 0$, $\tilde{R}_u = 2.74$, $\tilde{C}_{dl} = 0.0037$, $\Delta\tilde{E} = 4.0$, and $\tilde{\omega} = 16\pi$ were used to generate the synthetic data.

5.1 Choice of parameter values in AC Voltammetry

In comparing the information content in the DC and AC signals above we have used a single set of (non-dimensional) parameter values to generate the AC signals ($\tilde{\omega} = 16\pi$ and $\tilde{\Delta E} = 4.0$). In this section we justify this choice by demonstrating how changes in these two parameters affect the degree of accuracy in the recovered parameters. In all cases we use a standard deviation of the Gaussian noise of $\sigma = 0.5\%$ of the maximum current.

In Figure 7 we give the recovered posterior distributions for $\tilde{k}_0$, $\tilde{\alpha}$, $\tilde{C}_{dl}$ and $\tilde{R}_u$ as the frequency of the sinusoidal oscillation is varied from $\tilde{\omega} = 4\pi$ to 32π, using a value of $\tilde{\Delta E} = 4.0$ in each case (i.e. a large amplitude case). In Table 4 we give the corresponding values of the means of these distributions and the standard deviations about these mean values (in the table we also include the recovered distribution for $\tilde{E}_0$). For comparison, we also include in the first row of Table 4 the equivalent values for the DC signal. As can be seen, for all values of $\tilde{\omega}$, the standard deviation of the recovered distribution is much smaller than for the DC case. In both the AC and DC case, the parameter that is most affected by experimental noise is $\tilde{k}_0$, and it can be seen that the accuracy of the recovery of this parameter increases with increasing $\tilde{\omega}$ up to $\tilde{\omega} = 16\pi$; by this point the s.d. of the recovered distribution for $\tilde{k}_0$ is just 0.2% of the true value. To improve the value further we would need to improve the numerical accuracy of the underlying solution to the partial differential equation. For example, in the case of $\tilde{\omega} = 64\pi$, we doubled the number of timesteps used in solving Eq. 5 with the result that the standard deviation on all recovered parameters decreased with, for example, that for $\tilde{k}_0$ decreasing to 0.0056.

$\tilde{\omega}$	$\tilde{k}_0$ (s.d.)	$\tilde{\alpha}$ (s.d.)	$\tilde{C}_{dl}$ (s.d.) ($\times 10^3$)	$\tilde{R}_u$ (s.d.)	$\tilde{E}_0$
0	5.206 (0.2955)	0.5115 (0.0111)	3.718 (0.016)	2.741 (0.0105)	0.004621 (0.0039)
4π	5.028 (0.0296)	0.4992 (0.0009)	3.697 (0.002)	2.742 (0.0024)	-0.001325 (0.0005)
8π	5.083 (0.0204)	0.5011 (0.0009)	3.703 (0.001)	2.746 (0.0015)	0.000262 (0.0005)
16π	4.960 (0.0107)	0.4999 (0.0008)	3.703 (0.001)	2.738 (0.0007)	0.000802 (0.0006)
32π	5.013 (0.0078)	0.4997 (0.0008)	3.698 (0.001)	2.740 (0.0003)	0.000213 (0.0008)
64π	5.012 (0.0078)	0.4961 (0.0010)	3.699 (0.001)	2.739 (0.0002)	-0.000672 (0.0010)

Table 4: The effect of varying the frequency, $\tilde{\omega}$ of the AC oscillation on the mean and standard deviation of the recovered parameters. Note that the mean values are all very close to the true values used in generating the data (as expected). The key point to note is the change in the standard deviations about the mean values which are a direct measure of the effect of random noise on the value of the recovered parameter value. Standard deviations for the AC case are in all cases much lower than for the DC case. The default non-dimensional values of $\tilde{k}_0 = 5$, $\tilde{\alpha} = 0.5$, $\tilde{E}_0 = 0$, $\tilde{R}_u = 2.74$, $\tilde{C}_{dl} = 0.0037$, and $\tilde{\Delta E} = 4.0$, were used to generate the synthetic data.

The results in Table 4 justify our choice of $\tilde{\omega} = 16\pi$, whilst those in Figure 8 and Table 5 justify our choice of $\tilde{\Delta E} = 4.0$ (with, in these cases, all results being generated at a fixed value of $\tilde{\omega} = 16\pi$ and $\sigma = 0.5\%$ of the maximum current). Similarly to the variation with $\tilde{\omega}$, the accuracy of $\tilde{k}_0$ is the most dependent on $\tilde{\Delta E}$ and the improvements in the standard deviation of the recovered distribution increase with increasing $\tilde{\Delta E}$, but are tailing off by $\tilde{\Delta E} = 4.0$. In the next section, where we look at the effect of changing parameter values on the parameter recovery process, we restrict ourselves to comparing the DC case with the AC case using just this single set of values of $\tilde{\Delta E} = 4.0$ and $\tilde{\omega} = 16\pi$.

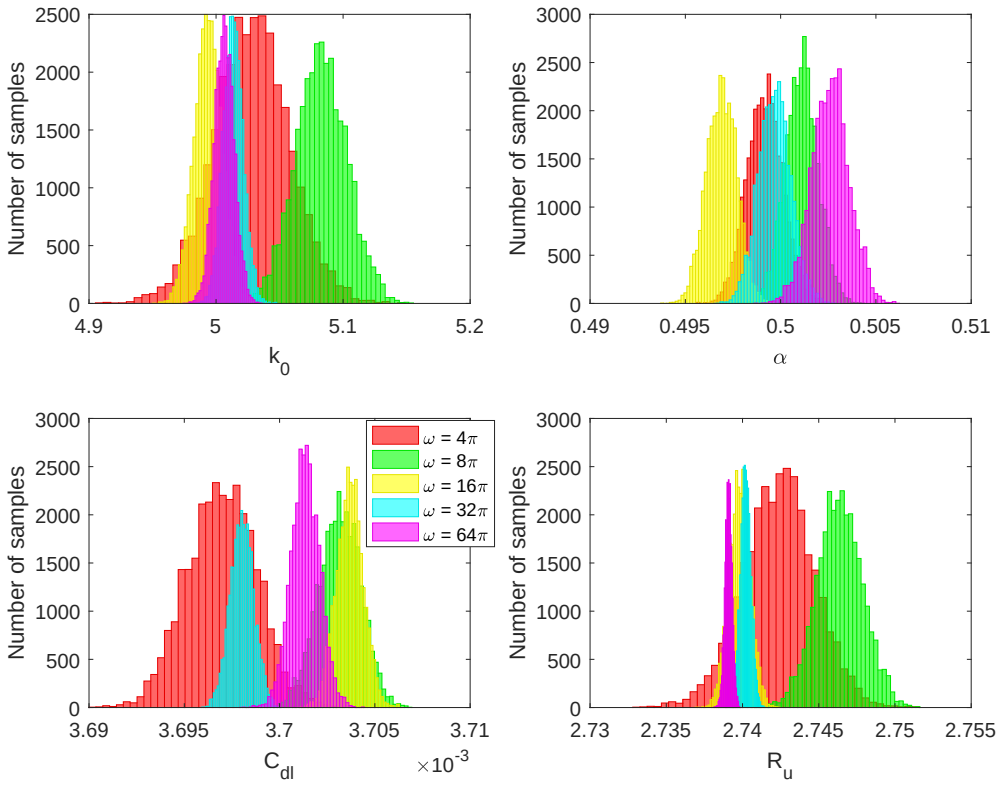

Figure 7: The effect of varying the frequency, $\tilde{\omega}$ of the AC oscillation on the recovered parameters distributions. The default non-dimensional values of $\tilde{k}_0 = 5$, $\tilde{\alpha} = 0.5$, $\tilde{E}_0 = 0$, $\tilde{R}_u = 2.74$, $\tilde{C}_{dl} = 0.0037$, and $\tilde{\Delta E} = 4.0$ were used to generate the synthetic data.

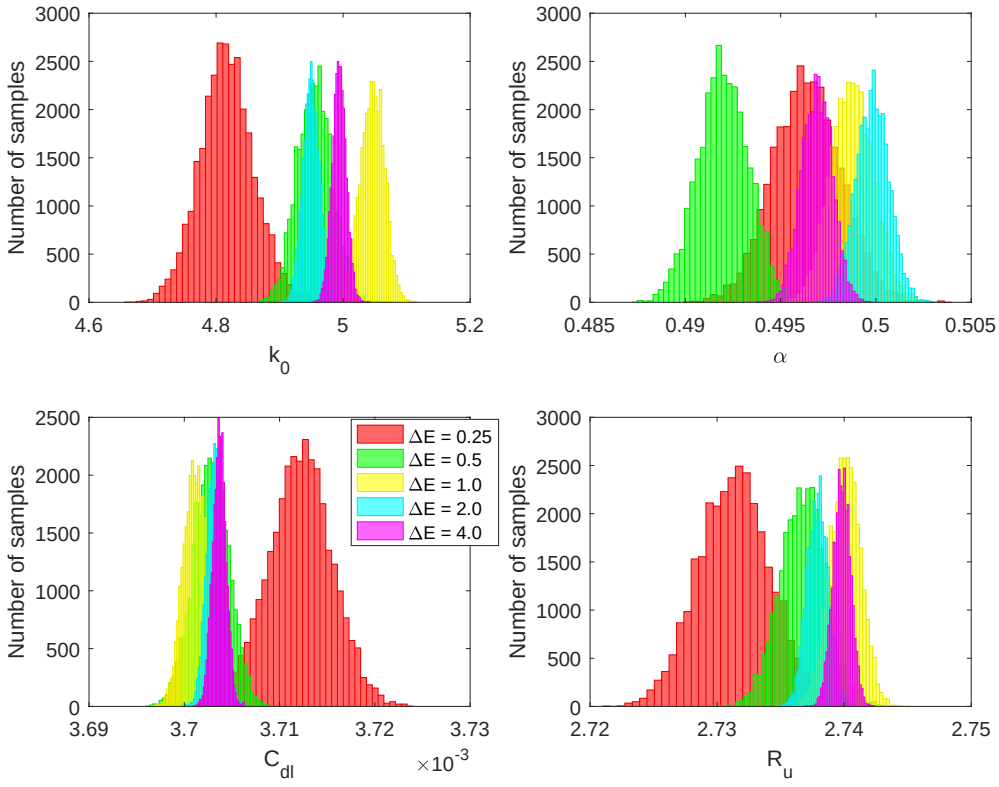

Figure 8: The effect of varying the amplitude, $\tilde{\Delta E}$ of the AC oscillation on the recovered parameters distributions.The default non-dimensional values of $\tilde{k}_0 = 5$, $\tilde{\alpha} = 0.5$, $\tilde{E}_0 = 0$, $\tilde{R}_u = 2.74$, $\tilde{C}_{dl} = 0.0037$, and $\tilde{\omega} = 16\pi$ were used to generate the synthetic data.

$\tilde{\Delta E}$	$\tilde{k_0}$ (s.d.)	$\tilde{\alpha}$ (s.d.)	$\tilde{C_{dl}}$ (s.d.) ($\times 10^3$)	$\tilde{R_u}$ (s.d.)	$\tilde{E_0}$
0.0	5.206 (0.296)	0.5115 (0.0111)	3.719 (0.0163)	2.742 (0.0104)	0.004621 (0.00400)
0.25	4.817 (0.043)	0.4964 (0.0017)	3.712 (0.0033)	2.731 (0.0028)	-0.001524 (0.00081)
0.5	4.955 (0.027)	0.4920 (0.0013)	3.703 (0.0019)	2.737 (0.0018)	-0.000854 (0.00062)
1.0	5.046 (0.019)	0.4988 (0.0011)	3.701 (0.0012)	2.740 (0.0012)	0.000528 (0.00059)
2.0	4.950 (0.013)	0.4998 (0.0009)	3.703 (0.0009)	2.738 (0.0009)	0.000436 (0.00061)
4.0	4.960 (0.011)	0.4999 (0.0008)	3.703 (0.0007)	2.738 (0.0007)	0.000802 (0.00066)

Table 5: The effect of varying the amplitude, $\tilde{\Delta E}$ of the AC oscillation on the recovered parameters distributions. The default non-dimensional values of $\tilde{k_0} = 5$, $\tilde{\alpha} = 0.5$, $\tilde{E_0} = 0$, $\tilde{R_u} = 2.74$, $\tilde{C_{dl}} = 0.0037$, and $\tilde{\omega} = 16\pi$ were used to generate the synthetic data.

5.2 Analysis of the effects of the electron transfer rate constant on the parameter recovery process

	$\tilde{k_0}$ (s.d.)	$\tilde{\alpha}$ (s.d.)	$\tilde{C_{dl}}$ (s.d.) ($\times 10^3$)	$\tilde{R_u}$ (s.d.)	$\tilde{E_0}$
DC	76.37 (18.50)	0.605 (0.061)	3.728 (0.002)	2.745 (0.0051)	0.0038 (0.0014)
AC	50.58 (1.22)	0.504 (0.007)	3.702 (0.0001)	2.740 (0.0008)	0.0012 (0.0006)

Table 6: The means and standard deviations of the recovered parameters for both the AC and DC cases using a value of $\tilde{k_0} = 50$ i.e. close to full reversibility. The default non-dimensional values of $\tilde{\alpha} = 0.5$, $E_0 = 0$, $\tilde{R_u} = 2.74$, $\tilde{C_{dl}} = 0.0037$, in both the AC and DC cases, and $\tilde{\Delta E} = 4.0$, and $\tilde{\omega} = 16\pi$ in the AC case, were used to generate the synthetic data.

The results that we have presented so far illustrate clearly that the parameter that is most affected by experimental noise is $\tilde{k_0}$, the electron transfer rate constant. This is perhaps not surprising since, as explained in the introduction, the value of $\tilde{k_0}$ determines the nature of the chemical process occurring at the electrode surface; as $\tilde{k_0}$ decreases it tends to an irreversible process, and as $\tilde{k_0}$ increases it tends to a fully reversible process. We would therefore expect that relatively high (particularly) or very low values of $\tilde{k_0}$ would cause difficulty for the parameter recovery technique since, for example, relatively large increases in $\tilde{k_0}$ result in only marginal changes in the measured current, as shown in Figure 2. In Table 6 and Figure 9 we show the results of attempting to recover the parameters from both the AC and DC signals using $\tilde{k_0} = 50$, i.e. close to full reversibility. As expected the recovered posterior distribution for $\tilde{k_0}$ is skewed to the right for the DC case and is much broader than the equivalent AC case - at these high values of $\tilde{k_0}$ it becomes increasingly difficult to determine $\tilde{k_0}$ as it has much less influence on the overall current, and this influence decreases further as $\tilde{k_0}$ continues to increase.

The recovery process for the parameters using the DC signal is also affected by parameter compensation (whereby the changes in two or more parameters can combine to have identical effects on the output signal and therefore cannot be distinguished) to a much greater degree; this is manifested by correlations in the changes between the recovered distributions of those parameters. This is clearly illustrated in Figures 10 and 11 which show the recovered distributions and the associated biplots for both the DC and AC signals respectively for $\tilde{k_0} = 50$. As can be seen, correlations are apparent between $\tilde{R_u}$

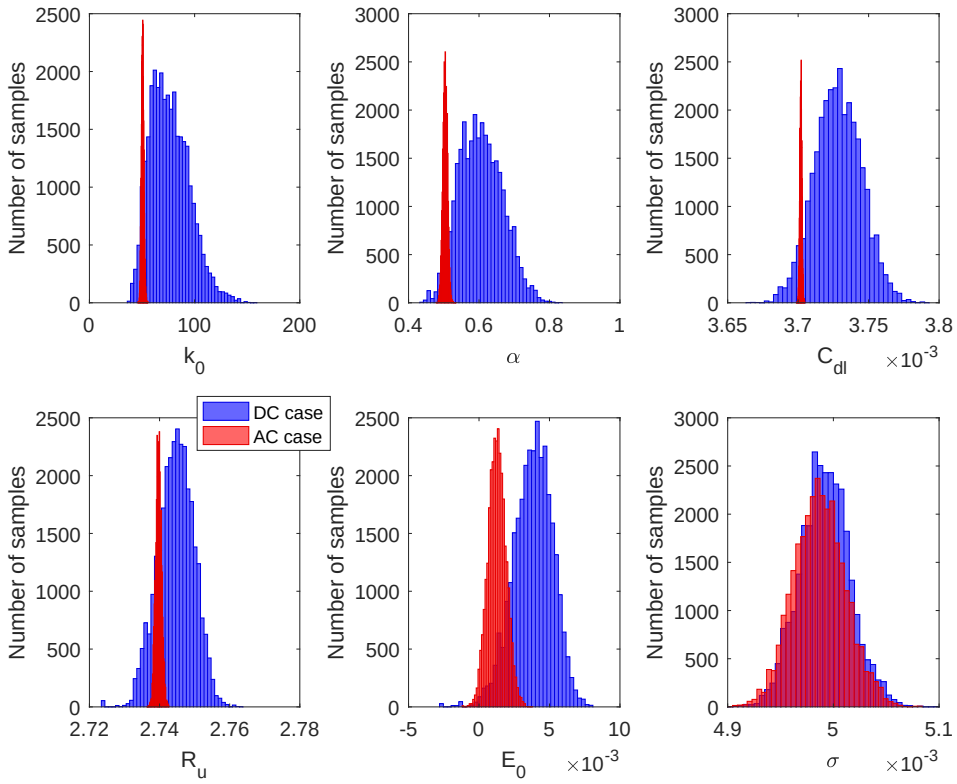

Figure 9: Comparison of the recovered posterior distributions for both the AC and DC cases using a value of $\tilde{k}_0 = 50$ i.e. close to full reversibility. The default non-dimensional values of $\tilde{\alpha} = 0.5$, $\tilde{E}_0 = 0$, $\tilde{R}_u = 2.74$, $\tilde{C}_{dl} = 0.0037$, in both the AC and DC cases, and $\Delta\tilde{E} = 4.0$, and $\tilde{\omega} = 16\pi$ in the AC case, were used to generate the synthetic data.

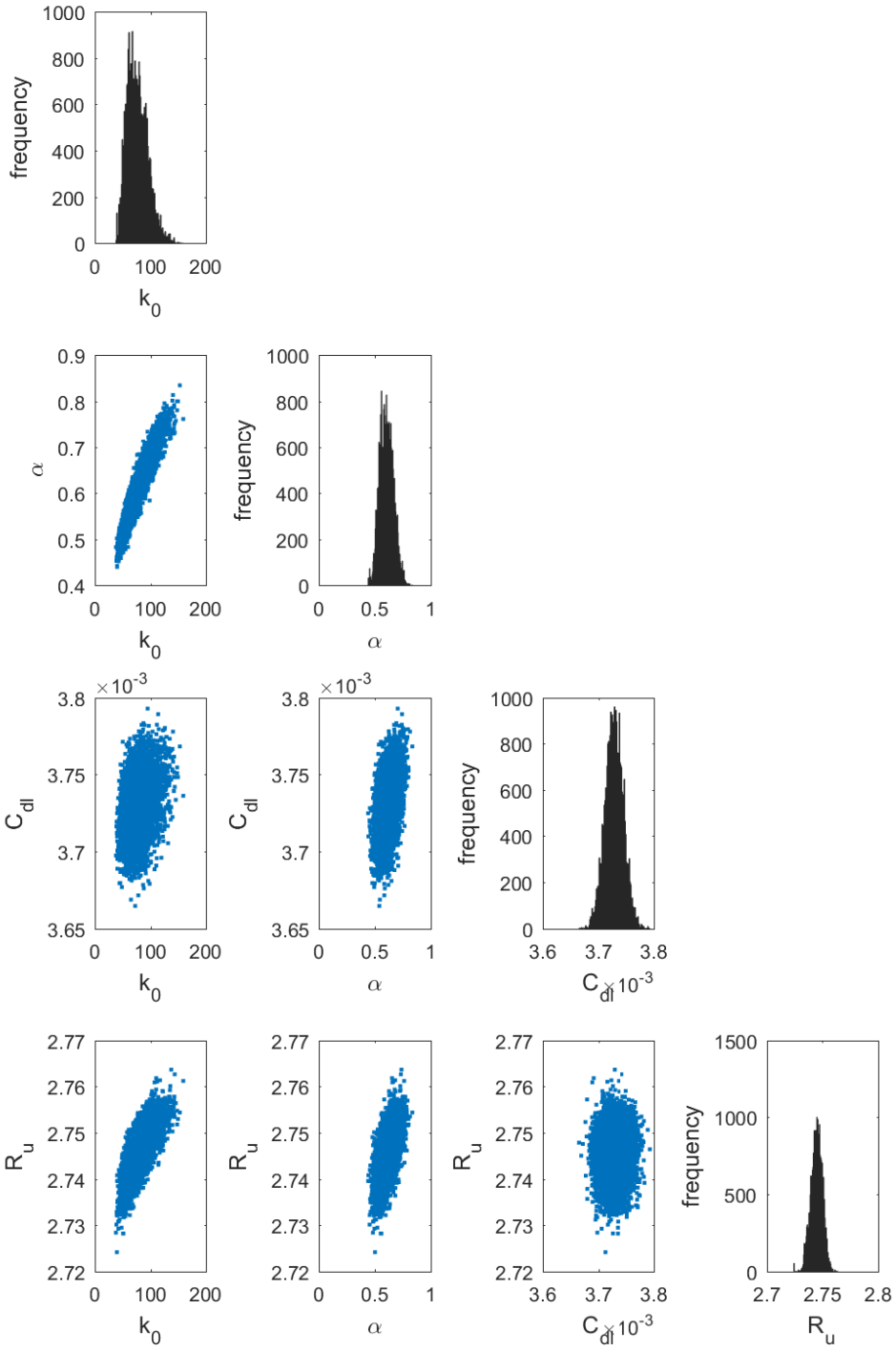

Figure 10: The recovered distributions and biplots for the DC case with $\tilde{k}_0 = 50$ demonstrating the appearance of parameter compensation as the fully reversible limit is approached. The default non-dimensional values of $\tilde{\alpha} = 0.5$, $\tilde{E}_0 = 0$, $\tilde{R}_u = 2.74$, $\tilde{C}_{dl} = 0.0037$ were used to generate the synthetic data.

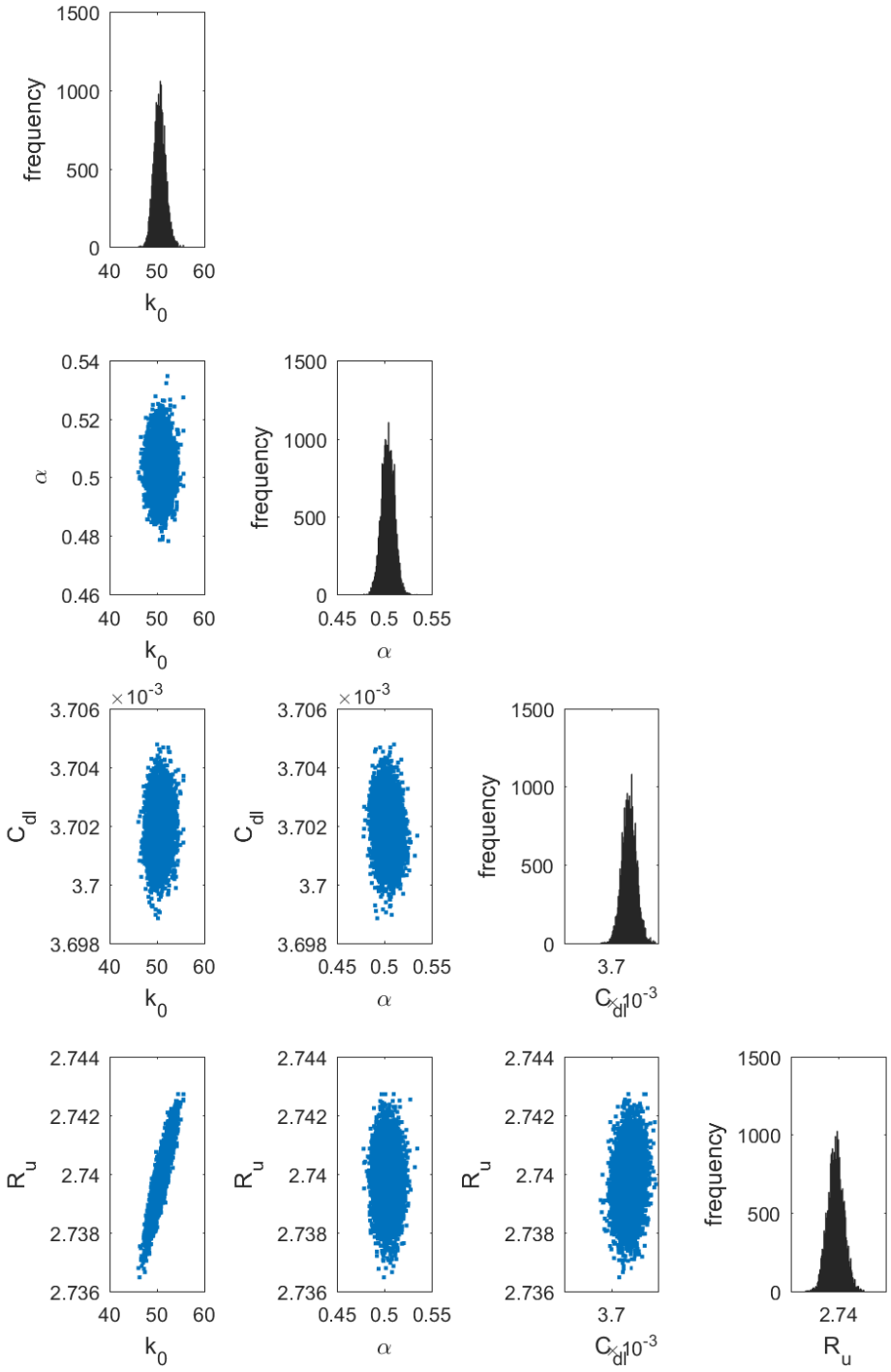

Figure 11: The recovered distributions and biplots for the AC case with $\tilde{k}_0 = 50$ demonstrating that the AC signal is affected to a much smaller degree by parameter compensation. The default non-dimensional values of $\tilde{\alpha} = 0.5$, $\tilde{E}_0 = 0$, $\tilde{R}_u = 2.74$, $\tilde{C}_{dl} = 0.0037$ and $\tilde{\Delta E} = 4.0$, and $\tilde{\omega} = 16\pi$ were used to generate the synthetic data.

and $\tilde{k}_0$, and $\tilde{\alpha}$ and $\tilde{E}_0$ in the recovered AC distributions, but these are still occurring over relatively tight intervals compared to the recovered DC distributions. For the DC signals, very strong correlations are beginning to appear between several pairs of parameters, with a particularly strong correlation emerging between $\tilde{k}_0$ and $\tilde{\alpha}$.

	$\tilde{k}_0$ (s.d.)	$\tilde{\alpha}$ (s.d.)	$\tilde{C}_{dl}$ (s.d.) ($\times 10^3$)	$\tilde{R}_u$ (s.d.)	$\tilde{E}_0$
DC	0.04997 (0.00071)	0.5006 (0.00047)	3.646 (0.0262)	2.725 (0.015)	-0.004272 (0.0272)
AC	0.04980 (0.00022)	0.4995 (0.00019)	3.700 (0.0004)	2.739 (0.005)	-0.002596 (0.0077)

Table 7: The means and standard deviations of the recovered parameters for both the AC and DC cases using a value of $\tilde{k}_0 = 0.05$ i.e. approaching the fully irreversible case. The default non-dimensional values of $\tilde{\alpha} = 0.5$, $\tilde{E}_0 = 0$, $\tilde{R}_u = 2.74$, $\tilde{C}_{dl} = 0.0037$, in both the AC and DC cases, and $\tilde{\Delta E} = 4.0$, and $\tilde{\omega} = 16\pi$ in the AC case, were used to generate the synthetic data.

Finally, we have also considered the case where $\tilde{k}_0$ is lowered so that the electrode process moves closer to irreversibility. Table 7 and Figure 12 summarise the recovered distributions from the DC and AC signals for this case, and Figures 13 and 14 give the corresponding biplots. In this case it can be seen that the recovered parameters for which there is the most dramatic improvement in using the AC rather than the DC signal are $\tilde{R}_u$ and $\tilde{C}_{dl}$, and for the first time $\tilde{E}_0$ also shows substantial improvement. The biplots again illustrate parameter compensation, with the correlations between $\tilde{E}_0$ and $\tilde{k}_0$ in the DC case being particularly striking.

6 Experimental results

As described in the methods section, in this paper we make a preliminary comparison of our theoretical work described above to a single experimental data set (data set 1) from reference [13]. We first non-dimensionalise that data set as described in the appendix, before re-dimensionalising to display the results. This allows us to use exactly the same simulation and parameter recovery algorithms (and software) to fit the experimental and synthetic data. In Figure 15 we show the results of using this same recovery procedure in analysing the results of two experimental data sets, one using an AC input signal and the other using a DC signal; other than the parameters used to generate the input signal, these two data sets use identical conditions in all respects (see section 2 above). To aid comparison between the widths of the data sets (which is our primary measure of the information content), the two histograms for each parameter have been centred around zero. As can be seen, we are able to recover distributions of values for all five experimental parameters from each of the data sets. It can be seen that a very similar pattern in terms of accuracy follows through for the experimental cases, with the width of the distributions for all parameters except E_0 being substantially narrower in the AC case. **However, note that the distribution for R_u is non-symmetric and gives values skewed towards zero; this indicates that for this particular experimental data set, R_u is indistinguishable from zero. Indeed we have re-fitted the data keeping R_u fixed at zero and have found that it has negligible effect on the recovery of the other parameters (data not shown).** In this publication we restrict ourselves (due to space considerations) to this brief qualitative validation of our theoretical results, leaving a more detailed quantitative comparison between experimental and synthetic (simulated

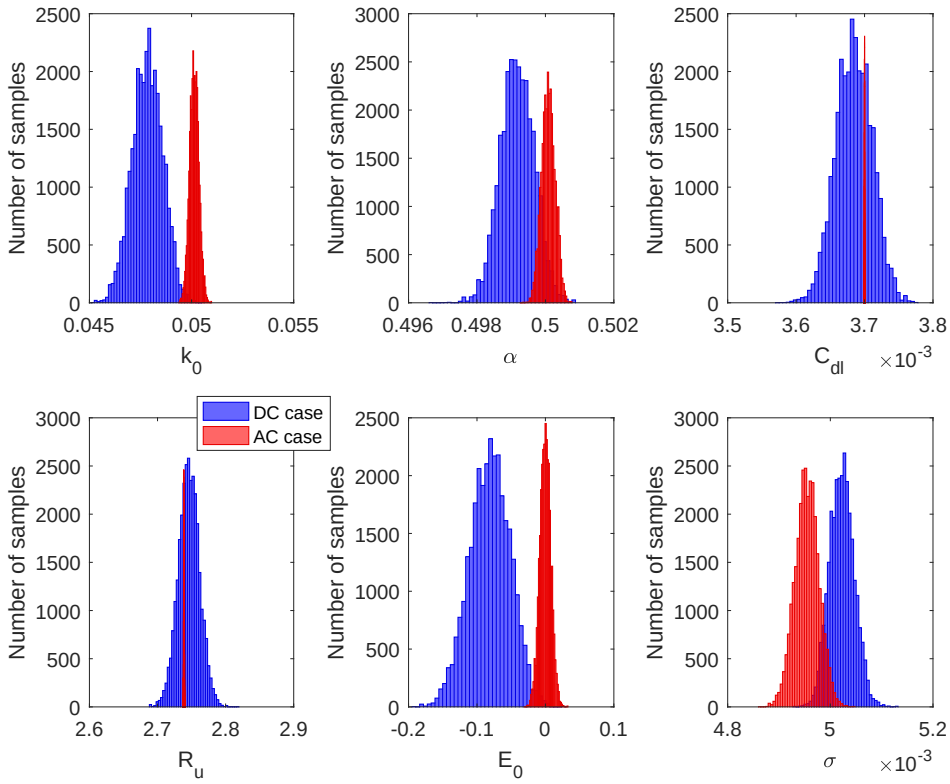

Figure 12: Comparison of the recovered posterior distributions for both the AC and DC cases using a value of $\tilde{k}_0 = 0.05$ i.e. close to full irreversibility. The default non-dimensional values of $\tilde{\alpha} = 0.5$, $\tilde{E}_0 = 0$, $\tilde{R}_u = 2.74$, $\tilde{C}_{dl} = 0.0037$, in both the AC and DC cases, and $\Delta\tilde{E} = 4.0$, and $\tilde{\omega} = 16\pi$ in the AC case, were used to generate the synthetic data.

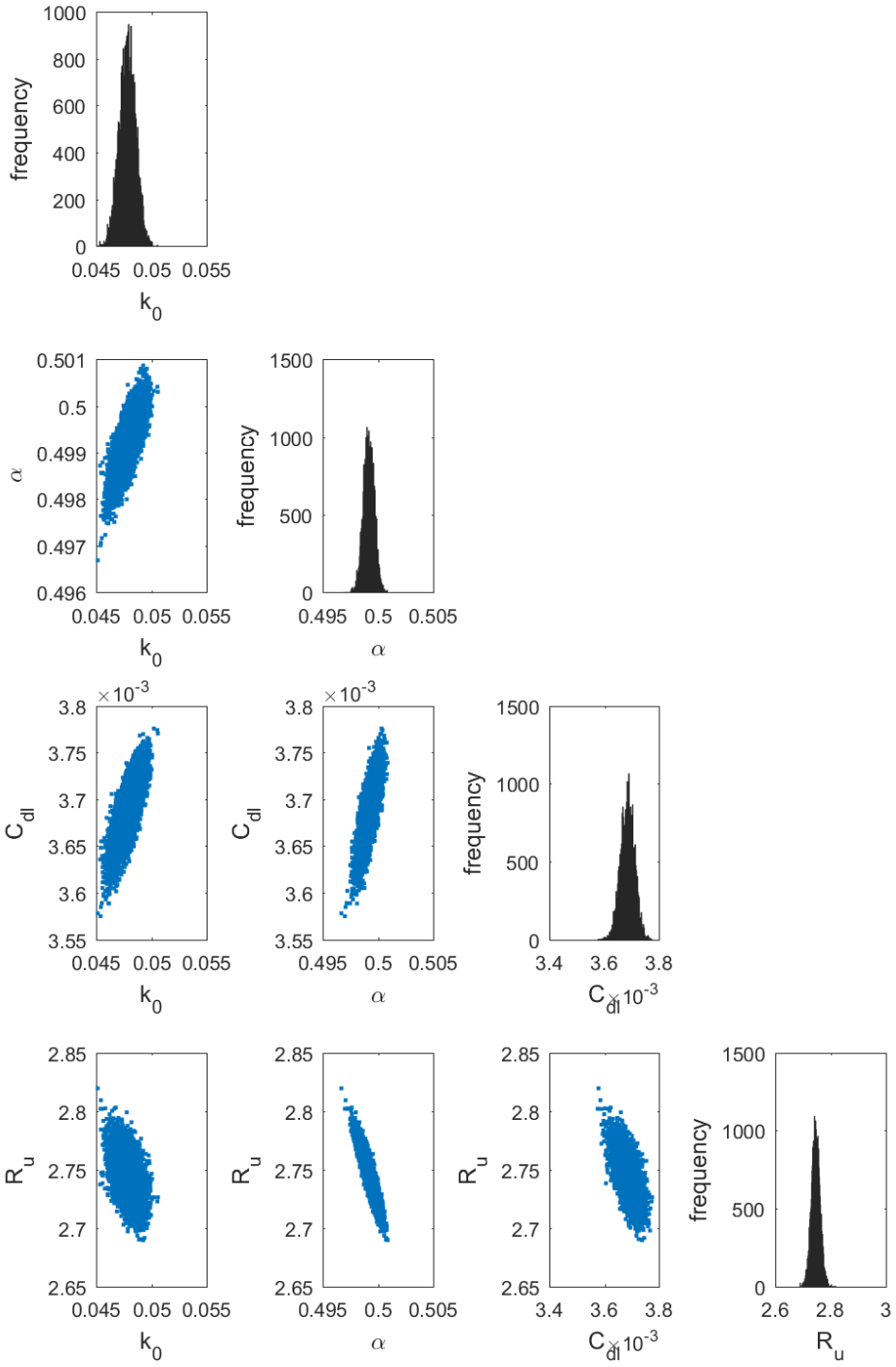

Figure 13: The recovered distributions and biplots for the DC case with $k_0 = 0.05$ demonstrating the appearance of parameter compensation as the fully irreversible limit is approached. The default non-dimensional values of $\tilde{\alpha} = 0.5$, $\tilde{E}_0 = 0$, $\tilde{R}_u = 2.74$, $\tilde{C}_{dl} = 0.0037$ were used to generate the synthetic data.

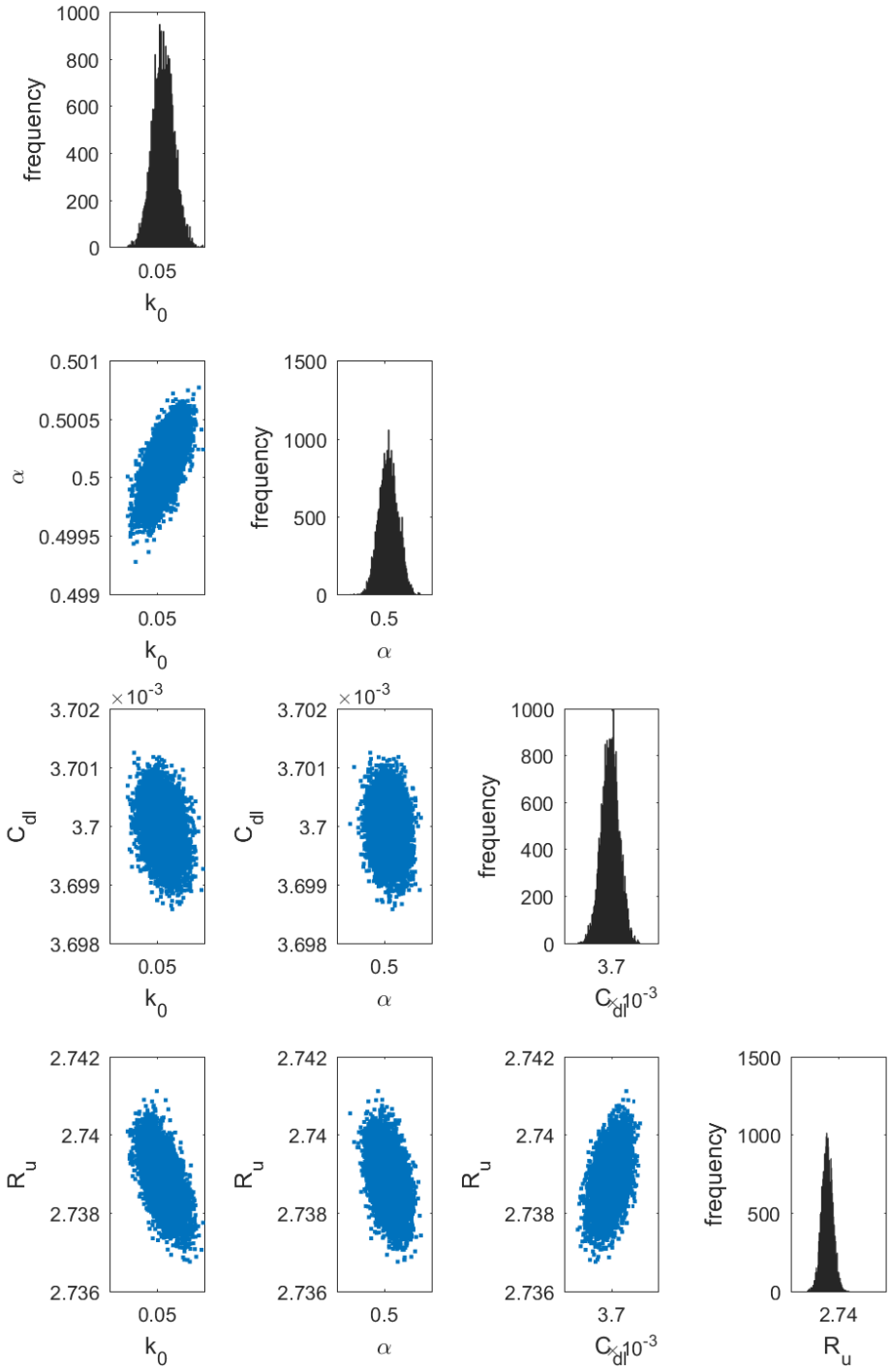

Figure 14: The recovered distributions and biplots for the AC case with $\tilde{k}_0 = 0.05$ demonstrating the appearance of parameter compensation as the fully irreversible limit is approached. The default non-dimensional values of $\tilde{\alpha} = 0.5$, $\tilde{E}_0 = 0$, $\tilde{R}_u = 2.74$, $\tilde{C}_{dl} = 0.0037$, and $\tilde{\Delta E} = 4.0$, and $\tilde{\omega} = 16\pi$ were used to generate the synthetic data.

data), and between the parameter values recovered from multiple repeats of the same experiment, to a future publication.

7 Conclusions

This detailed study, undertaken on the analysis of DC and AC voltammetric data confirms that Bayesian inference facilitates the reliable recovery of parameters relevant to the thermodynamics and electrode kinetics for a quasi-reversible process in the presence of uncompensated resistance and double layer charging current. The comparison also has established the extent to which even the simplest possible AC voltammetric method based on superimposition of a sine wave onto the DC potential ramp is advantageous. When the requisite inverse problem is addressed in a Bayesian framework supported by MCMC methods with simulated data containing experimentally realistic levels of noise, the recovered distribution for each of ($\tilde{k}_0$, $\tilde{\alpha}$, $\tilde{E}_0$, R_u and $\tilde{C}_{dl}$) is significantly narrower when the AC method is employed. The ability to accurately recover the electrode kinetic and thermodynamic parameters ($\tilde{k}_0$, $\tilde{\alpha}$, $\tilde{E}_0$), which is also affected by R_u and $\tilde{C}_{dl}$, as estimated by spreads of their distributions is shown to be a function of amplitude and frequency of the sine wave as well as the kinetic regime (closeness to reversible or irreversible limits of the quasi-reversible process) as well as R_u and $\tilde{C}_{dl}$. The significantly enhanced ability of the AC method to quantify faster electrode kinetics is related to the greatly enhanced dependence of current magnitude on $\tilde{k}_0$ and R_u as well as the dual AC and DC time scales.

A study based on experimental data derived from DC and AC voltammograms for the reduction of $[Fe(CN)_6]^{3-}$ to $[Fe(CN)_6]^{4-}$ supports the conclusions reached from analysis of simulated data containing known levels of noise. On this basis we now suggest that placing the electrode kinetic inverse problem in a Bayesian framework and exploiting the use of computational approaches based on MCMC methods to assess the accuracy with which the inverse problem can be solved for the electrode kinetic and other parameters should lead to significant advances in quantitative analysis of electrochemical data as has been found in other branches of science. In particular, whist this study addresses the impact of random noise only (i.e. the impact of random Gaussian experimental noise on the accuracy of the recovered parameters), a platform has now been established for the first time to separate uncertainties in parameter estimates arising from random noise arising within a single experiment as in this study, and that due to the variability within the system that can only be assessed using multiple (replicate) experiments. This framework will also allow us to assess the impact of any inadequacies in the modelling that could, for example, arise from use of the Butler-Volmer Model rather than Marcus-Hush electron transfer relationships [1, 4] to describe the electron transfer process.

We will reserve for a future paper the consideration of multiple repeats of the same experiment under identical laboratory conditions. This future work will enable a distinction to be made between the effects of random experimental noise and those due to the inherent variability of the system, and to quantify the degree of variability in the electrochemical process. Thus we will be in a position (for the first time to our knowledge in electrochemistry) to separate out the effects of experimental noise from the inherent variability arising in repeated experiments. This will allow us to demonstrate how much variation in recovered parameter values we might anticipate between repeated runs of the same experiment, and to estimate the absolute accuracy with which it might be possible to estimate parameters such as the electron transfer rate constant, charge transfer

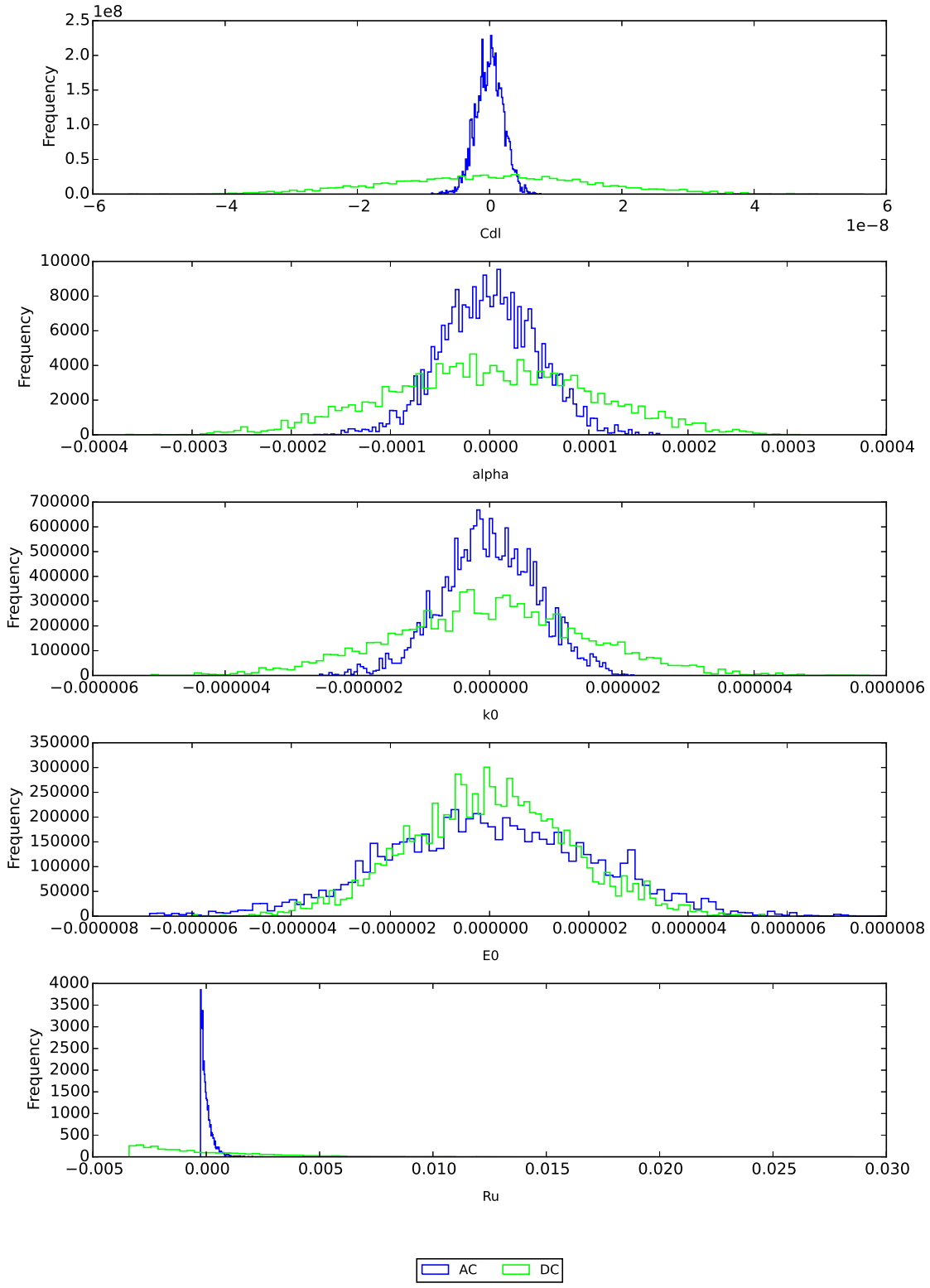

Figure 15: Comparison of the recovered posterior distributions for both the AC and DC cases from the experimental data. The distributions are centred about zero to facilitate comparison of the relative width of the distributions.

coefficient, or reversible potential from voltammetric experiments.

Acknowledgements

AMB, DJG and JZ would like to acknowledge the support Australian Research Council through the award of a Discovery Grant DP170101535. ACD gratefully acknowledges funding by the Rhodes Trust, UK. J.C. gratefully acknowledges research support from the '2020 Science' programme funded through the EPSRC Cross-Disciplinary Interface Programme (EP/I017909/1). CG gratefully acknowledges from the EPSRC Doctoral Training Grant EP/G037280/1.

8 Keywords

Voltammetry, Inverse Problems, Bayesian Inference, Parameter Estimation, Confidence Limits

9 TOC

Bayesian inference is shown to be a powerful technique for assessing information content of voltammetric experiments. The approach yields distributions of parameter values (see 16) and hence estimates of the accuracy of recovered parameters. AC voltammetry is shown to yield parameters with much greater accuracy that its DC counterpart.

References

[1] A. Bard, L. Faulkner, *Electrochemical Methods: Fundamentals and Applications*, John Wiley & Sons, Inc, **2001**.

[2] C. Brett, A. Brett, Oliveira, *Principles, Methods, and Applications of Electrochemistry*, **1993**.

[3] D. Pletcher, R. Greff, R. Peat, L. Peter, J. Robinson, *Instrumental methods in electrochemistry*, Elsevier, **2001**.

[4] R. Compton, C. Banks, *Understanding voltammetry*, World Scientific, **2011**.

[5] A. Simonov, G. Morris, E. Mashkina, B. Bethwaite, K. Gillow, R. Baker, D. Gavaghan, A. Bond, *Anal. Chem.* **2014**, *86*, 8408–8417.

[6] H. Matsuda, Y. Ayabe, *Ber. Bunsenges. Phys. Chem* **1955**, *59*, 494–503.

[7] A. Bond, D. Elton, S.-X. Guo, G. Kennedy, E. Mashkina, A. Simonov, J. Zhang, *Electrochem. Comm.* **2015**, *57*, 78–83.

[8] A. Bond, *Modern polarographic methods in analytical chemistry*, *Vol. 4*, CRC Press, **1980**.

[9] A. M. Bond, N. W. Duffy, S.-X. Guo, J. Zhang, D. Elton, *Anal. Chem.* **2005**, *77*, 186 A–195 A.

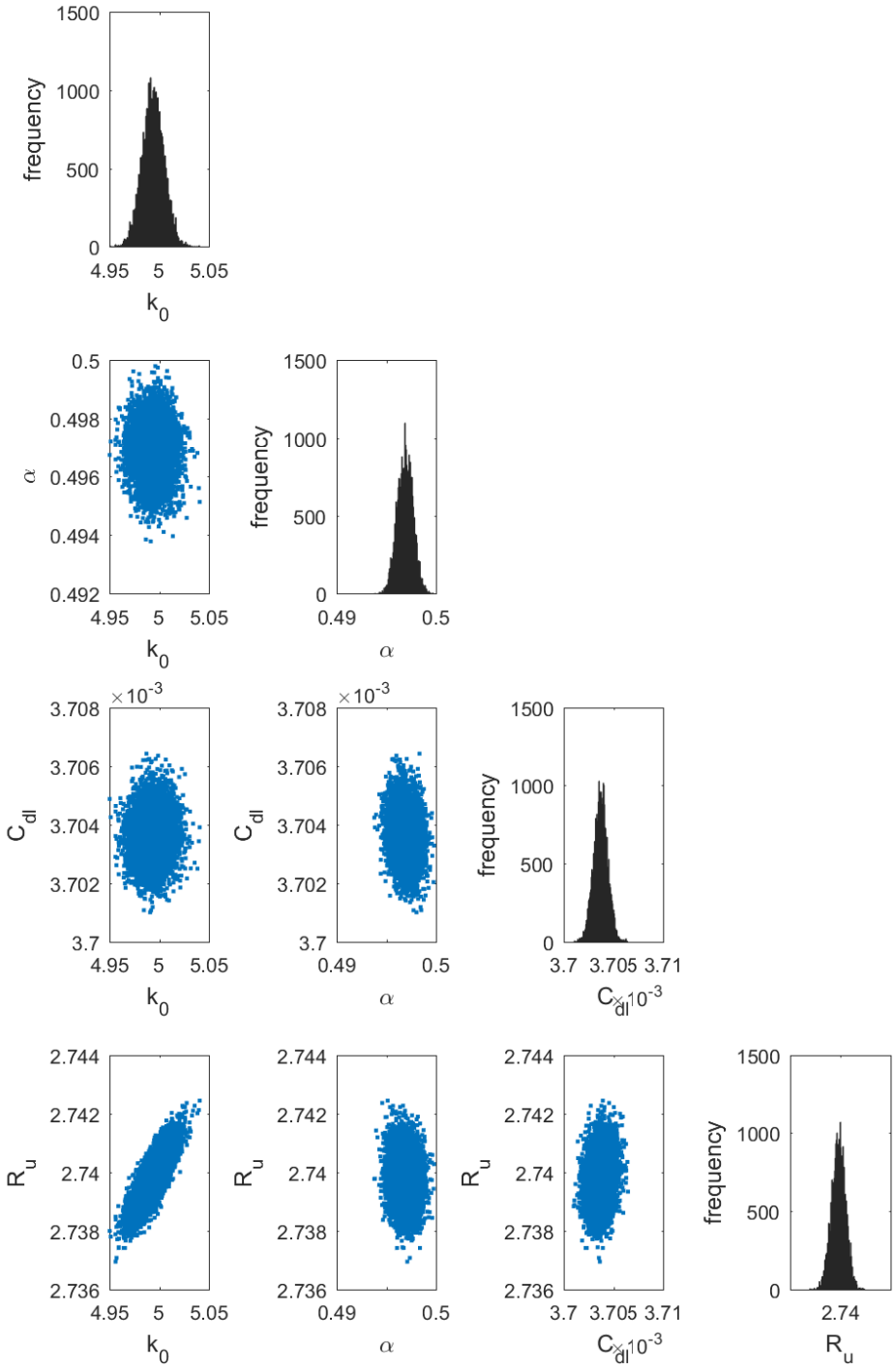

Figure 16

[10] S.-X. Guo, A. Bond, J. Zhang, *Rev. Polarogr.* **2015**, *61*, 21–32.

[11] D. Gavaghan, A. Bond, *Electroanalysis* **2006**, *18*, 333–344.

[12] A. Sher, A. Bond, D. Gavaghan, K. Harriman, S. Feldberg, N. Duffy, S.-X. Guo, J. Zhang, *Anal. Chem.* **2004**, *76*, 6214–6228.

[13] G. Morris, A. Simonov, E. Mashkina, R. Bordas, K. Gillow, R. Baker, D. Gavaghan, A. Bond, *Anal. Chem.* **2013**, *85*, 11780–7.

[14] A. Sher, A. Bond, D. Gavaghan, K. Harriman, S. Feldberg, N. Duffy, S.-X. Guo, J. Zhang, *Anal. Chem.* **2004**, *76*, 6214–28.

[15] A. Bond, E. Mashkina, A. Simonov, *Developments in Electrochemistry: Science Inspired by Martin Fleischmann* **2014**, 21–47.

[16] L. Bieniasz, B. Speiser, *J. Electroanal. Chem.* **1998**, *458*, 209–229.

[17] L. Bieniasz, H. Rabitz, *Anal. Chem.* **2006**, *78*, 8430–8437.

[18] N. Armstrong, D. Hibbert, *Chemom. Intell. Lab. Syst.* **2009**, *97*, 194–210.

[19] R. Johnstone, E. Chang, R. Bardenet, T. De Boer, D. Gavaghan, P. Pathmanathan, R. Clayton, G. Mirams, *J. Mol. Cell. Cardiol.* **2016**, *96*, 49–62.

[20] D. Hibbert, N. Armstrong, *Chemom. Intell. Lab. Syst.* **2009**, *97*, 211–220.

[21] J. Samuel, *Empirical Models for Cyclic Voltammograms*, University of Southampton, **2010**.

[22] X. Zhu, J. Wang, B. Li, *JDCTA* **2010**, *4*, 123–131.

[23] M. Bogdan, D. Brugger, W. Rosenstiel, B. Speiser, *J. Cheminf.* **2014**, *6*, 30.

[24] http://www.nag.co.uk.

[25] J. Rice, *Mathematical statistics and data analysis*, Nelson Education, **2006**.

[26] W. Hastings, *Biometrika* **1970**, *57*, 97–109.

[27] W. Gilks, S. Richardson, D. Spiegelhalter, *Markov Chain Monte Carlo in Practice*, London: Chapman and Hall, **1996**.

[28] H. Haario, E. Saksman, J. Tamminen, *Bernoulli* **2001**, 223–242.

[29]

[30] D. Gavaghan, A. Bond, *J. Electroanal. Chem.* **2000**, *480*, 133–149.

[31] R. Bardenet, *IN2P3 School of Statistics (SOS2012)* **2013**, *55*, year.

[32] A. Gelman, J. Carlin, H. Stern, D. Dunson, A. Vehtari, D. Rubin, *Bayesian data analysis*, CRC Press, Boca Raton, FL, 3rd ed., **2014**, pp. xiv+661.

[33] G. O. Roberts, J. S. Rosenthal, *Stat. Sci.* **2001**, *16*, 351–367.

Supplementary Information

S1 Non-dimensionalising the equations

Let $u = c_A/c_\infty$ and $\tilde{E}_{DC} = \theta(E_{DC}) = \theta(E_{start}+vt)$, where $\theta = \frac{F}{RT}$. We non-dimensionalise time t and the sweep rate v according to

$$\tilde{t} = t\theta v, \tag{S1}$$

$$\tilde{v} = v\frac{t_{final}}{E_{DC}(t_{final}) - E_{DC}(0)} = 1. \tag{S2}$$

Let $\tilde{x} = x/\ell$, where $\ell = D^{1/2}(\theta v)^{-1/2}$. Changing variables in equation (5) gives

$$\frac{\partial u}{\partial \tilde{t}} = \frac{\partial^2 u}{\partial \tilde{x}^2}.$$

Transforming equation (7) into non-dimensional variables gives

$$I_f(t) = FSc_\infty (\theta D v)^{1/2} \left(\frac{\partial u}{\partial \tilde{x}}\right)_{\tilde{x}=0}.$$

Thus, we arrive at the non-dimensional faradaic current.

$$\tilde{I}_f(\tilde{t}) = \left(\frac{\partial u}{\partial \tilde{x}}\right)_{\tilde{x}=0}, \tag{S3}$$

where $\tilde{I}_f(\tilde{t}) = \left(FSc_\infty (\theta D v)^{1/2}\right)^{-1} I_f(t)$.

When non-dimensionalising the period, frequency, and sinusoidal potential we follow the approach of [30]. We aim to impose the alternating potential as $\tilde{E}_{AC} = \Delta\tilde{E}\sin(\tilde{\omega}\tilde{t})$. Let N be the number of oscillations in the timescale, as this must remain fixed after non-dimensionalising. Importantly, $\tilde{t}_{final}$ is equal to the range of $\tilde{E}_{DC}$, and therefore, also equal to θE_{range} where E_{range} is the range of E_{DC}. In dimensional variables $t_{final} = E_{range}/v$. The dimensional and non-dimensional periods are thus

$$P = \frac{t_{final}}{N} = \frac{E_{range}}{vN}, \text{ and } \tilde{P} = \frac{\tilde{t}_{final}}{N} = \frac{\theta E_{range}}{N},$$

respectively. Thus, $P = (v\theta)^{-1}\tilde{P}$. The dimensional and non-dimensional frequencies ω and $\tilde{\omega}$ satisfy $\omega = \frac{2\pi}{P}$ and $\tilde{\omega} = \frac{2\pi}{\tilde{P}}$, so in particular

$$\frac{\omega}{\tilde{\omega}} = \frac{\tilde{P}}{P} = v\theta.$$

It follows that

$$\tilde{\omega} = (v\theta)^{-1}\omega.$$

Now, the ratio of the amplitude of the AC potential, and the range of the DC potential must be the same after non-dimensionalising. That is

$$\frac{\Delta\tilde{E}}{\tilde{E}_{range}} = \frac{\Delta E}{E_{range}},$$

$$\tilde{E}_{DC} = \theta E_{AC}, \qquad \tilde{x} = \left(D^{-1}\theta v\right)^{1/2} x,$$
$$\Delta\tilde{E} = \theta \Delta E, \qquad u = \left(\frac{1}{c_\infty}\right) c_A,$$
$$\tilde{E} = \theta E, \qquad \tilde{t} = (\theta v)\, t,$$
$$\tilde{\omega} = (\theta v)^{-1}\, \omega,$$
$$\tilde{k}_0 = (\theta D v)^{-1/2}\, k_0, \qquad \tilde{C}_{dl} = v^{1/2} \left(F S c_\infty (\theta D)^{1/2}\right)^{-1} C_{dl},$$
$$\tilde{R}_u = \left(\theta F S c_\infty (\theta D v)^{1/2}\right) R_u, \qquad \tilde{I}_f = \left(F S c_\infty (\theta D v)^{1/2}\right)^{-1} I_f.$$

Table S1: The relation between dimensional and non-dimensional variables in the model

it follows that $\Delta\tilde{E}_{DC} = \theta(\Delta E)$.

The remaining parameters are non-dimensionalised by considering the relation $I_C = C_{dl}\frac{dE_{eff}}{dt}$ and that the effective potential is $E_{eff} = E_{app} - I_{tot}R_u$ where $E_{app} = E_{DC} + E_{AC}$. We summarise the relation between the dimensional and non-dimensional variables in Table S1.

The following equations describe the model in non-dimensional variables:

$$\frac{\partial u}{\partial \tilde{t}} = \frac{\partial^2 u}{\partial \tilde{x}^2}. \tag{S4}$$

The total current output is $\tilde{I}_{tot} = \tilde{I}_f + \tilde{I}_C$, where $\tilde{I}_C = \tilde{C}_{dl}\frac{d\tilde{E}_{eff}}{d\tilde{t}}$, and

$$\tilde{I}_f = \tilde{k}_0 \left(u(0,t)e^{(1-\alpha)(\tilde{E}_{eff}-\tilde{E}_0)} - (1-u(0,t))e^{-\alpha(\tilde{E}_{eff}-\tilde{E}_0)}\right). \tag{S5}$$

Boundary and initial conditions are given by

$$\tilde{x} = 0: \qquad \frac{\partial u}{\partial \tilde{x}} = \tilde{I}_f(\tilde{t});$$
$$\tilde{x} \to \infty: \qquad u = 1;$$
$$\tilde{t} = 0: \qquad u = 1.$$

Here, $\tilde{E}_{app} = \tilde{E}_{DC} + \tilde{E}_{ac}$ and $\tilde{E}_{eff} = \tilde{E}_{app} - \tilde{I}_{tot}\tilde{R}_u$, where

$$\tilde{E}_{DC} = \frac{F}{RT}E_{start} + \tilde{t}; \text{ and}$$
$$\tilde{E}_{AC} = \Delta\tilde{E}\sin(\tilde{\omega}\tilde{t}).$$

S2 The Metropolis-Hastings Algorithm

As described in section 3.5, in sampling from the posterior distribution for $\boldsymbol{\theta}$ we make use of a Markov Chain Monte-Carlo (MCMC) approach implemented by using the Metropolis-Hastings algorithm. Typically when using MCMC samplers, a 'burn-in' period is introduced within which the proposal distribution can be tuned, and the sampler should find its way to a region of parameter space with high density. In this way, the effect of the

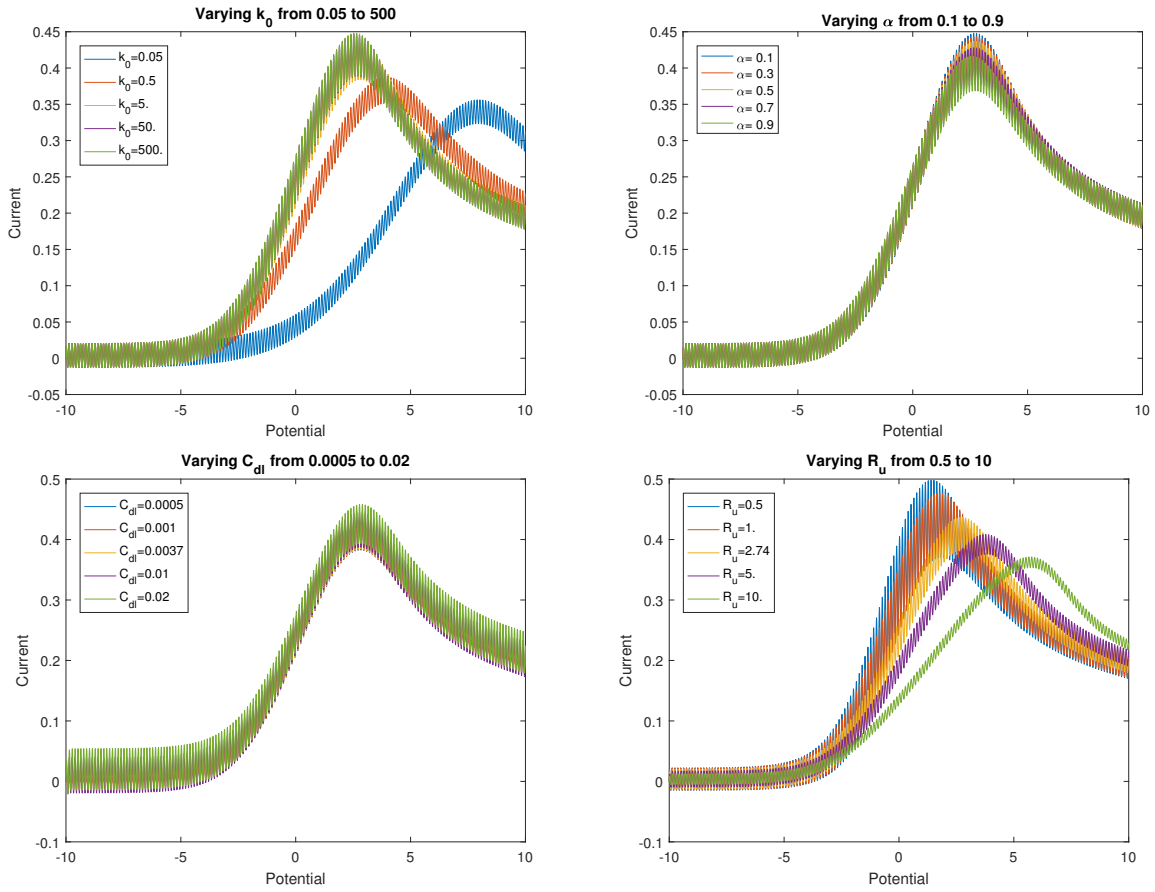

Figure S1: The above plots show the effect of changing individual parameters in simulated currents from numerical solution of the model equations in response to a linear sweep dc potential. All parameters are $\tilde{k}_0 = 5, \tilde{\alpha} = 0.5, \tilde{E}_0 = 0, \tilde{C}_{dl} = 0.0037$, and $\tilde{R}_u = 2.74$, unless indicated otherwise.

initial start point of the chain is removed. If the proposal distribution is too wide then it can be the case that lots of steps are rejected and it takes a long time for the chain to explore parameter space, and similarly, if the distribution is too narrow then the acceptance rate will be high, but the parameter space will not be explored sufficiently during the finite time of the run. In practice, an acceptance rate of approximately 0.25 is considered optimal for parameter space of dimension at least 2. This value has been shown to be optimal for Gaussian proposal and posterior distributions, but has been accepted more widely as a rule of thumb in the literature [31, 32, 33].

In the approach that we have implemented, we make use of a multivariate Gaussian proposal distribution, centered at the previous sample point, and utilise an adaptive covariance matrix method as described in [31], based on [28]. Our adaptive Metropolis-Hastings sampler of [28] follows the same basic principle as a Metropolis-Hastings sampler described in section 3.5 using a multivariate Gaussian as the proposal distribution, but it also continuously updates the covariance matrix within the proposal distribution by approximating the covariance of the full history of the chain at each step. With this adaptivity, the chain is no longer strictly Markov, but retains the correct ergodic convergence properties [28]. We used a slight adaptation of this method following [31] in which the adjustment of the covariance matrix is reduced at each step, with the chain constructed in such a way as to select the desired overall acceptance rate.

The pseudocode in Algorithm 1 gives the algorithm we have employed. It samples proposed value of the parameters of interest (in our case $\boldsymbol{\theta} = (\tilde{k}_0,\ \tilde{\alpha},\ \tilde{E}_0,\ \tilde{R}_u,\ \tilde{C}_{dl},\ \sigma)$, where σ is the standard deviation of the normally distributed noise that is also estimated as part of the inverse problem) from a multivariate Gaussian distribution centred at the previous sample point (lines 7 and 22). Initially (lines 6-19) this proposal distribution has a fixed covariance matrix during a run in period, before switching (lines 20 to 38) to using a proposal distribution with a covariance matrix that is adaptively refined to ensure the desired acceptance rate of 25% (with the adaptivity implemented in lines 34 to 36). In all instances in this paper, the diagonal matrix D used in the run in phase (line 4) is calculated as one third of the width of the prior distribution for each parameter. The accepted sample values from the posterior distribution (the $\boldsymbol{\theta_t}$) are the outputs from the algorithm, and it is these values that are visualised as histograms in the results presented in the paper. To ensure that the MCMC algorithm is efficient in terms of computational time, we have initiated all MCMC simulations at the global optimum of the likelihood found by minimizing equation (18) using either the `cma-es` or the `fminsearch` algorithms available in Matlab [29]. In this way, we make use of the efficient optimization algorithms to explore parameter space, locating the mode of the posterior distribution and use MCMC to sample locally from the posterior distribution. The burn-in period is therefore only needed in order to allow the chain to converge, and the adaptive covariance method to achieve the desired acceptance rate. Typically, we ran the chain for 40000 steps and discarded the first 10000 samples as burn-in.

Algorithm 1 The adaptive covariance MCMC algorithm used to generate the results throughout the paper.

Set $a_0 = 1$.
Set $\boldsymbol{\theta_0}$ as determined by global optimization using either CMA-ES or fminsearch.
Set $\boldsymbol{\mu_0} = \boldsymbol{\theta_0}$.
Set $\Sigma_0 = D$, where D is a suitable diagonal matrix.
$t := 1$
while $t \leq 1000\times$(number of parameters) **do**
  Given the current parameter state $\boldsymbol{\theta_t}$, sample $\boldsymbol{\theta^*} \sim \mathcal{N}(\boldsymbol{\theta_t}, a_0\Sigma_0)$.
  if $p(\boldsymbol{\theta^*}) \neq 0$ **then**
    Compute $r = \exp(l(\boldsymbol{\theta^*}|\mathbf{y}) - l(\boldsymbol{\theta_t}|\mathbf{y}))$.
    Sample $u \sim \mathcal{U}(0, 1)$.
    if $u < r$ **then**
      Set $\boldsymbol{\theta_{t+1}} = \boldsymbol{\theta^*}$.
    else
      Set $\boldsymbol{\theta_{t+1}} = \boldsymbol{\theta_t}$.
    end if
  else
    Set $\boldsymbol{\theta_{t+1}} = \boldsymbol{\theta_t}$.
  end if
  t++ i.e. increment t by 1
end while
loop
  Set $s = t - 1000\times$(number of parameters).
  Set $\gamma_s = (s + 1)^{-0.6}$.
  Given the current parameter state $\boldsymbol{\theta_t}$, sample $\boldsymbol{\theta^*} \sim \mathcal{N}(\boldsymbol{\theta_t}, a_{s-1}\Sigma_{s-1})$.
  if $p(\boldsymbol{\theta^*}) \neq 0$ **then**
    Compute $r = \exp(l(\boldsymbol{\theta^*}|\mathbf{y}) - l(\boldsymbol{\theta_t}|\mathbf{y}))$.
    Sample $u \sim \mathcal{U}(0, 1)$.
    if $u < r$ **then**
      Set $\boldsymbol{\theta_{t+1}} = \boldsymbol{\theta^*}$.
      Set $accepted = 1$.
    else
      Set $\boldsymbol{\theta_{t+1}} = \boldsymbol{\theta_t}$.
      Set $accepted = 0$.
    end if
  else
    Set $\boldsymbol{\theta_{t+1}} = \boldsymbol{\theta_t}$.
    Set $accepted = 0$.
  end if
  Set $\Sigma_s = (1 - \gamma_s) \times \Sigma_{s-1} + \gamma_s \times (\boldsymbol{\theta_{t+1}} - \boldsymbol{\mu_{s-1}})^T(\boldsymbol{\theta_{t+1}} - \boldsymbol{\mu_{s-1}})$.
  Set $\boldsymbol{\mu_s} = (1 - \gamma_s) \times \boldsymbol{\mu_{s-1}} + \gamma_s \times \boldsymbol{\theta_{t+1}}$.
  Set $a_s = \exp(\log(a_{s-1}) + \gamma_s \times (accepted - 0.25))$.
  t++ i.e. increment t by 1
end loop